DEVELOPMENT OF MULTIFUNCTIONAL DENDRITIC POLYMERS FOR INJECTABLE BONE TISSUE ENGINEERING

Final Report Submitted to Department of Biotechnology (DBT), Government of India

(DBT Sponsored Twinning Project Grant No. BT/235/NE/TBP/2011 Dated April 30, 2012)

Submitted by

Niranjan Karak, Tapas K Maiti, Satyabrat Gogoi, Somnath Maji and Birendra Behera

DEPT. OF CHEMICAL SCIENCES
TEZPUR UNIVERSITY
NAPAAM, 784028
ASSAM, INDIA

DEPT. OF BIOTECHNOLOGY
INDIAN INSITUTE OF TECHNOLOGY
KHARAGPUR, 721302
WEST BENGAL, INDIA

September, 2015

DEVELOPMENT OF MULTIFUNCTIONAL DENDRITIC POLYMERS FOR INJECTABLE BONE TISSUE ENGINEERING

Final Report Submitted to Department of Biotechnology (DBT), Government of India

(DBT Sponsored Twinning Project Grant No. BT/235/NE/TBP/2011 Dated April 30, 2012)

Submitted by

Niranjan Karak, Tapas K Maiti, Satyabrat Gogoi, Somnath Maji and Birendra Behera

DEPT. OF CHEMICAL SCIENCES
TEZPUR UNIVERSITY
NAPAAM, 784028
ASSAM, INDIA

DEPT. OF BIOTECHNOLOGY
INDIAN INSITUTE OF TECHNOLOGY
KHARAGPUR, 721302
WEST BENGAL, INDIA

September, 2015

Content

SECTION A

PROJECT DETAILS

Section-A: Project Details

A1. Project Title:	Development of Multifunctional Dendritic Polymers for Injectable Bone Tissue Engineering
A2. DBT Sanction Order No. & Date:	BT/235/NE/TBP/2011 dated April 30, 2012
A3. Name of Principal Investigator:	Professor Niranjan Karak
Name of Co-PI/Co-Investigator:	Professor Tapas Kumar Maiti
A4. Institute:	North-East Institute: Tezpur University Collaborating Institute: IIT, Kharagpur
A5. Address with Contact Nos. (Landline & Mobile) & Email:	Department of Chemical Sciences Tezpur University Napaam, 784028, Assam, India Mobile No.- +91 9957184354 Email : karakniranjan@yahoo.com & Department of Biotechnology Indian Institute of Technology-Kharagpur Kharagpur, West Bengal-721302 Mobile No.-+91 9474597751 E-mail; tkmaiti@hijli.iitkgp.ernet.in
A6. Total Cost:	64.22 lakhs (TU) + 37.10 (IITKharagpur)
A7. Duration:	3 years

A8. Approved Objectives of the Project:

- Synthesis and characterization of biocompatible dendritic polymers using natural amino acid back bone and their biological characterization. Selection of specific peptides (TU).
- Standardization of conjugation chemistry for covalent linking of one or more peptides and phyico-chemical characterization of the conjugates (TU). Cytocompatibility testing of the conjugates (IITKgp).
- Conjugation of self assembling peptides and study of its *in situ* gelling properties (TU).
- Study of cellular response towards the multifunctional polymers in vitro in terms biochemical signaling pathway using tissue specific cells (IITKgp).
- In vitro bone formation study in 3D and subsequent *in vivo* evaluation (IITKgp).

SECTION B

SCIENT5IFIC AND TECHNICAL PROGRESS

B 1. DEVELOPMENT OF MULTIFUNCTINAL DENDRTIC POLYMERS FOR INJECTABLE BONE TISSUE ENGINEERING

1. Introduction

With the advances in the field of regenerative medicine the development of novel biocompatible material has gained a great deal of interest. The current scenario of increasing number of organ failure and demand of their subsequent replacement has triggered mounting interest to search out suitable biomaterials [1, 2]. As a result, tissue engineered materials have emerged out with hopes and promises. However, bone repair and regeneration of bone tissues still remain as challenge due to clinical complexities [3, 4]. Bone defect due to trauma, infections, tumors or congenital disorders become common cases across the globe [5]. The major impediment associated with the bone treatment is the lake of efficiency to regenerate itself [6]. Henceforth, apposite endoprosthetic replacement is required in the treatment of such irreparable injury in order to facilitate the defect site requisite physiological functions [7]. Such prostheses must be bioactive so that they can promote and support the infiltration of bone cells or other related biomolecules and accelerate their adhesion and proliferation. Therefore, designing and fabrication of novel scaffold material lodge a major area in the domain of biomaterial research.

In this context, polymeric prosthesis has been extensively mentioned in literature [8-10]. The tunable characteristics like mechanical strength, porosity, microstructure, degradability, size and shape make polymeric materials suitable for tissue engineering application [11]. However, synthetic matrices often lack cell-recognition signals found in naturally derived materials, resulting in less effective seeding of the cells onto the matrix [7]. This seems to over shadow the wide spectrum of polymers to fulfil the requirement of target specific *in vivo* bone treatment. Moreover, such material associates with the concern of host reaction due to xenobiotic nature. Therefore, improvement of bioactivity of such material is necessary. In this regard, bio-nano functionalization of biocompatible polymers by utilizing the knowledge of material science, nanotechnology and biological science can create ample opportunities towards an efficient prosthesis with efficient cytocompatibility, osteoblast proliferation and differentiation ability. In this milieu, peptides appear to be an appropriate

molecule for bio-fabrication. Peptides can act as an ideal interface to bridge between synthetic and biological systems [12]. Many peptides have been reported to stimulate osteoblast adhesion, migration, proliferation and differentiation [13-17].

Thus, in the present investigation attempts have been made to conjugate four different types of peptides *viz.* SVVYGLR (SR-7, angiogenic peptide), PRGDSGYRGDS (PS-11, cell adhesion peptide), IPP (IP-3, osteoblast differentiating peptide) and CGGKVGKACCVPTKLSPISVLYK (CK-23, osteogenic peptide) to a waterborne hyperbranched polyurethane matrix. Polyurethane being a mechanically robust, biocompatible and biodegradable material has been mentioned in the literature time and again for its numerous biomedical applications [18-21]. Moreover, hyperbranched architectural features confer many unique material properties such as low viscosity, large number of multifunctional groups with enhanced protein absorption ability etc. Abovementioned peptides are conjugated with multifunctional carbon nano dot by following sulpho-NHS coupling method. Having bestowed with remarkable cytocompatibility, nano carbon dots have been used extensively for bio-medical applications like bio-imaging, drug and gene delivery etc. [22-25]. These surface-passivated bio-nanohybrids have been used to fabricate the polyurethane matrix *ex situ*. Carbon dot acts as a solid support for the peptides as well as acts as nano-reinforcing agent to enhance the mechanical strength of the polymer. So, derived bio-nano-polymer composite is used as a scaffold material after modifying with 10 wt% of gelatin. *In vivo* and *in vitro* evaluation of cytocompatibility, osteoblast proliferation and differentiation has been performed to explore the aptness of this material for endoprosthetic replacement.

2. Objectives

- Synthesis and characterization of biocompatible dendritic polymers using natural amino acid block and their biological characterization. Selection of specific peptides (TU).
- Standardization of conjugation chemistry for covalent linking of one more peptides and physico-chemical characterization of the conjugates (TU). Cytocompatibility test of the conjugates (IIT, Khg).
- Conjugation of self-assembly peptides and study of its *in situ* gelling properties (TU).

- Study of cellular response towards the multifunctional polymers *in vitro* in terms of biochemical signaling pathways using tissue specific cells (IIT, Khg).
- *In vitro* bone formation study in 3D and subsequent *in vivo* evaluation (IIT, Khg).

3. Work done during the period

3.1. Synthesis of waterborne hyperbranched polyurethane (WHPU) using tannic acid as the branched moiety

Since its inception, polyurethane has emerged as the material of interest in colossal domains owing to its versatile properties. Polyurethane has been extensively mentioned in literature as biomaterial over and again due to its cytocompatibility and adequate biodegradability. Chemically, polyurethane is a condensation product of di/poly isocyanate with di/polyol. The most attractive feature about polyurethane is its tunable material properties; which can be achieved by altering the structure and composition of the raw materials, varying the NCO/OH ratio etc. Although, conventional polyurethanes possess good cytocompatibility, but challenges like high volatile organic compound content (VOC) and xenobiotic behavior of traditional solvent borne polymeric materials have posed a serious nuisance over their applications as biomaterials. Hence, waterborne polyurethane was synthesized using tannic acid as a bio-based component. Use of tannic acid as a bio-based component is an interesting alternative because of its renowned bioactivity, radical scavenging ability and peptide binding ability. Moreover, it provides a perfectly branched structure for the formation of a hyperbranched polymeric architecture.

3.1.1. Synthesis

In the first step isophorone diisocyanate (IPDI), poly(ethylene glycol)-600 (PEG) and bis-methyl propionic acid (BMPA) were taken in a three neck reactor equipped with a nitrogen inlet, a mechanical stirrer and an oil bath at NCO/OH ratio equal to 1.5. Reaction was carried out at 80-90 °C for 2 h. In the next step tannic acid (TA) and 1,4-butane-diol (BD) were introduced to the reactor such that NCO to OH ratio becomes 1. Tetrahydrofuran was used as a low boiling point solvent. Reaction was carried out for 5 h at temperature 65-70 °C. Then temperature was reduced (up to room temperature) and triethyl amine (TEA) was slowly added with constant mechanical stirring for 45 min. In the final step water was

added. THF was removed under reduced pressure to get polyurethane in water. WHPU was synthesized using different weight percentages of TA; detail composition is listed in **Table 1**.

Table 1. Composition of WHPUs

	Composition	WHPU05	WHPU10	WHPU15
IPDI	(mol)	2.00	2.00	2.00
PEG 600	(mol)	0.80	0.80	0.80
BMPA	(mol)	0.53	0.53	0.53
BD	(mol)	0.60	0.54	0.50
TA	(mol)	0.04	0.07	0.11
TEA	(mol)	0.53	0.53	0.53
NCO/OH (functional ratio)		1.00	1.00	1.00

3.1.2. Characterization

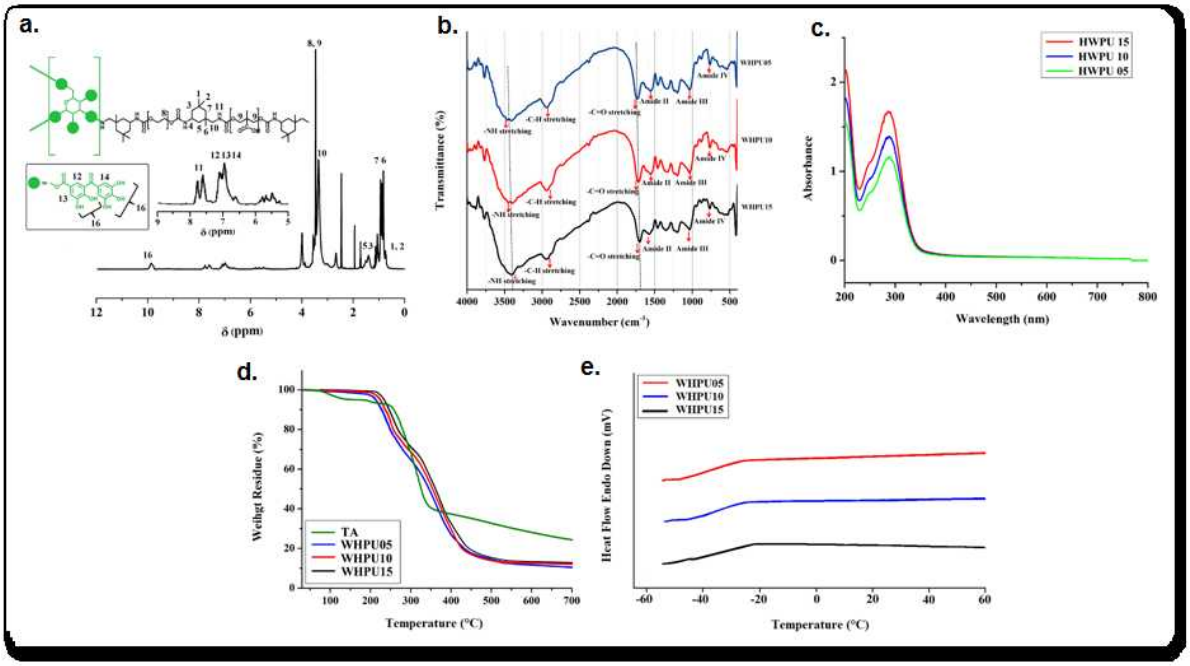

Figure 1. a. ^{1}H NMR**, b.** FTIR and **c.** UV-visible spectra of WHPU; d. TGA thermograms and **e.** Glass transition temperatures of WHPUs.

The structural confirmation of the synthesized WHPU was done by ^{1}H NMR, FTIR and UV-visible analyses. The spectra depicted in (**Figure 1.a, b, c**) confirmed the structure of the polymer.

FTIR (cm^{-1})	3490-4000 (O–H stretching); 1720-1735 (C=O); 1600-1605 (aromatic C=C); 1572 (N–H bending); 1108 (N–H deformation); 773-779 amide IV (in and out deformation); 631-635 amide V (in and out deformation). The observed frequencies established the different functional groups present and also confirmed the formation of urethane linkage. Shift in IR frequency for N-H and C=O group indicates formation of hydrogen bonding within the polymer structure.
^{1}H NMR (ppm)	δ 0.86-0.89 [- (C**H$_2$**) n-]; δ 1.5-0.7 [C**H$_2$** and C**H$_3$** of aliphatic cyclohexyl ring system], δ 3.4 [-C**H$_2$**-NH-C(=O)-O- belonging to IPDI]; δ 3.4 [-CH_2-C**H$_2$**-O-C(=O)- and $(CH_3)_2$C-C**H$_2$**-O-C(=O)]; δ 6.8-7.2 [aromatic proton Ar-**H**]; δ 7.7-7.9 [*cis* and *trans* urethane proton-N**H**-C(=O)-O-], δ 10.0 [phenolic protons Ph-O**H**]. The chemical shift values indicate various protons present in different chemical environment in the polyurethane structure. Further, formation of urethane linkage was confirmed.
UV-Visible spectroscopy	Absorbance peak at 280 nm due to the catechol fraction of tannic acid.

3.1.3. Physical properties

The number average, weight average molecular weight, poly disparity index (PDI) and solution viscosity of WHPUs were determined and tabulated below (**Table 2**).

Table 2. Weight average (M_w), number average (M_N) molecular weight; polydispersity index (PDI) and solution viscosity of WHPU compositions

Composition	WHPU05	WHPU10	WHPU15
M_W (g mol^{-1})	22,600	23,300	25,700
M_N (g mol^{-1})	16,200	18,900	21,700
PDI	1.39	1.23	1.34
Solution viscosity (dL/g)	0.365	0.298	0.274

3.1.4. Material properties (Thermal and mechanical)

Thermogravimetric analysis (TGA) showed two step degradation profiles for the polymer compositions (**Figure 1.d**). With increase in tannic acid content thermal stability also increases. On the other hand, glass transition temperature also increases with increase in tannic acid content (**Figure 1.e**).

WHPU 05 T_{ON} = 270; T_{END} = 443; T_{MAX} 310; T_g= -24.8

WHPU 10 T_{ON} = 273, T_{END} = 448, T_{MAX} 320; T_g = -22.2

WHPU 15 T_{ON} = 277, T_{END} = 459; T_{MAX} 327; T_g = -21.4

On the other hand, the synthesized polymer exhibited acceptable mechanical strength. Tensile strength is found to increase with TA content in the polymer. The mechanical properties are tabulated in **Table 3**.

Table 3. Mechanical properties of WHPU compositions

Composition	WHPU05	WHPU10	WHPU15
Tensile strength (MPa)	4.93	6.02	6.87
Elongation at break (%)	508 ± 5	457 ± 7	315 ± 4
Scratch hardness (kg)	4.0	5.0	5.5
Gloss (60 °)	98.7 ± 0.7	94.5 ± 0.8	88.2 ± 0.4

3.2. Selection of peptides for conjugation

To impart more signal specific bioactivity to the above synthesized WHPU matrix peptides are conjugated. In this context, synthetic peptides come into the picture. Compared to a whole protein, peptides are good candidates for conjugation with a hyperbranched polymer because of minimal steric hindrance faced. Literature reveals various peptides of bone and non-bone origin for stimulating osteoblast adhesion, proliferation and differentiation. We have *in-silico* selected four different peptides with specific function for bone tissue engineering (**Table 4**).

Table 4. List of peptides

PEPTIDES (Abbreviation used)	**FUNCTION**	**SOURCE**
SVVYGLR (SR-7)	Angiogenic peptide	Osteopontin
PRGDSGYRGDS (PS-11)	Cell Adhesion Peptide	RGD binding sequence
IPP (IP-3)	Osteoblast differentiation	Fermented Milk
CGGKVGKACCVPTKLSPISVLYK(CK-23)	Osteogenic peptides	Human BMP-9

3.3. Bio-nano conjugation of Carbon Dot (CD) with peptides

In order to conjugate the peptides to the WHPU matrix, an efficient strategy is short out by synthesizing a novel bio-nano hybrid of peptides with Carbon Dot (CD). Here, it is pertinent to mention that CD is the most recent addition to the carbon nano family admired many attractive properties. This carbon based quantum dot exhibits excellent water solubility with remarkable biocompatibility. Henceforth, it has been widely reported for various biomedical applications like drug delivery, bio-imaging, biosensor etc. Thus, such a cytocompatible and water soluble multifunctional bio-nano hybrid can be effectively used for the bio-fabrication of synthetic WHPU matrix.

3.3.1. Synthesis of CD

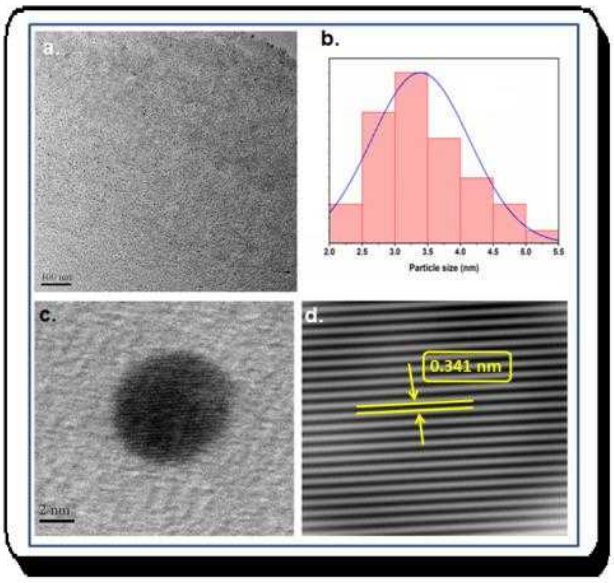

Figure 2. a. TEM image of CD, **b.** Size distribution of CD, **c.** HRTEM of CD and **d.** IFFT of HRTEM of CD

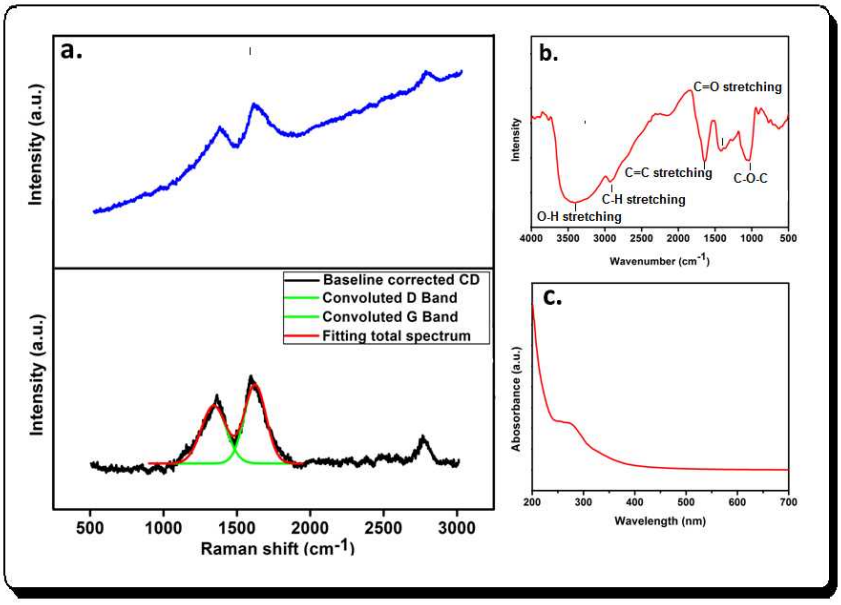

Figure 3. a. Raman spectrum (before and after base line correction), **b.** FTIR spectrum and **c.** UV-visible spectrum of CD.

CD was synthesized by hydrothermal method using corm of *Colocasia esculenta* as a bio-based raw material. Aqueous extract of corms of *C. esculenta* was prepared. Approximately 50 mL of this extract was poured into a 150 mL stainless steel autoclave with Teflon lining and subjected to thermal treatment at 170 °C for 5 h. A dark brown colored solution of CD

was obtained. To separate the large particles, solution was centrifuged at 960 × g (3000 rpm) for 15 min. Water was removed under reduced pressure to get CD in a semi-solid state. The formation of CD was confirmed by TEM images (spherical morphology, average size 3.2 nm, size distribution 2.2.-5.8 nm, spacing 0.341 nm) as shown in **Figure 2**. **a, b, c** and **d**. UV visible spectroscopy (absorption peak at wavelength 265 nm) and Raman spectroscopy (appearance of D and G band at 1365 cm^{-1} and 1584 cm^{-1} respectively, 2D band at 2849 cm^{-1}) (**Figure 3**) further ensured the formation of CD.

3.3.2. Bio-conjugation of CD/peptide

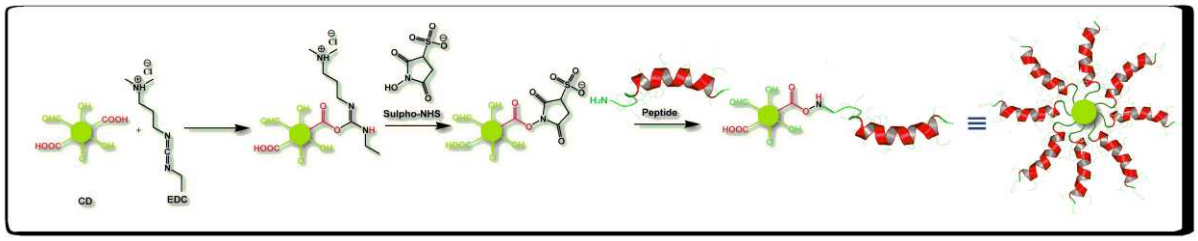

Scheme 1: CD/peptide bio-conjugation

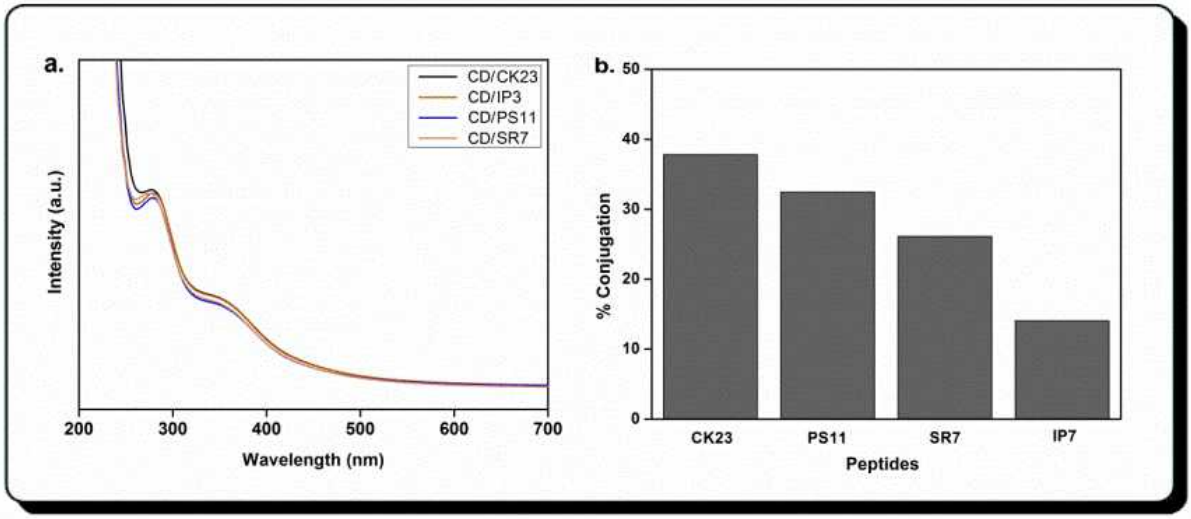

Figure 4. a. UV-visible spectra of CD/peptide bio-nanohybrid and **b.** percentage conjugation of various peptides with CD.

CD and peptide conjugation was achieved by succinimide coupling method (EDC-NHS) as shown in **Scheme 1**. Briefly, CD solution (1 mg/mL) was sonicated in an ice bath using a probe-type sonicator under a power of 40 W for 1 h. Then 5 mM of Sulfo-NHS, 1 mM of EDC were added into the CD solution and the mixture was bath sonicated for 1 h. Then, 1 mM of

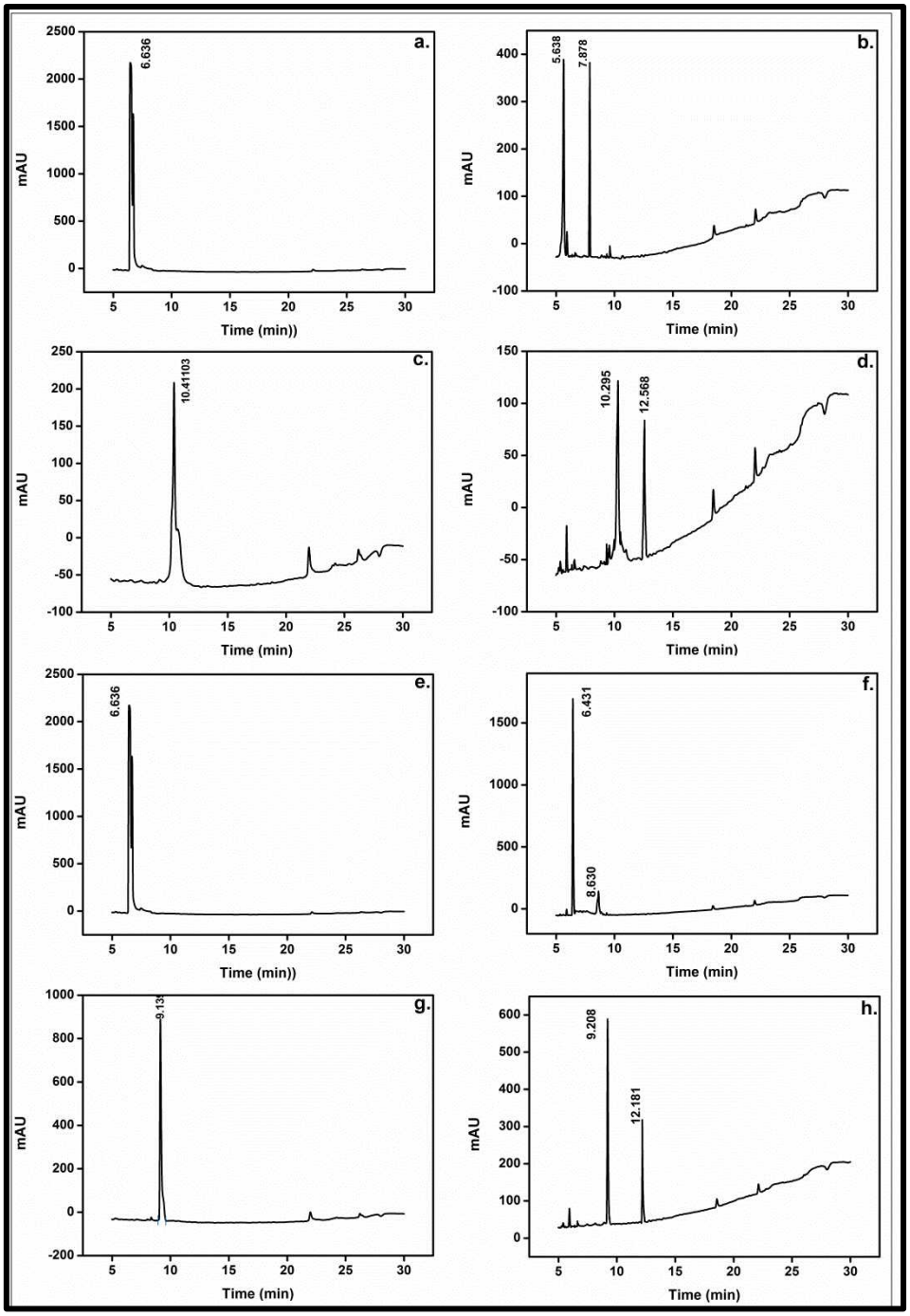

Figure 5. HPLC results for bio-conjugation of CD/peptide.

each peptide was added to the CD solution and stirred vigorously for overnight in an ice bath. The conjugation was confirmed by HPLC method and UV-visible spectroscopic analyses (**Figure 4. a and Figure 5**). CD with various forms bio-nanohybrid of CD and peptide thus obtained was stored at 4 °C. The RP-HPLC result shows that more than 30% of CK23 and PS11 peptide has conjugated with the CD where as conjugation percentage is low for the peptide IP3 (**Figure 4.b**).

3.4. Bio-fabrication of waterborne hyperbranched polyurethane

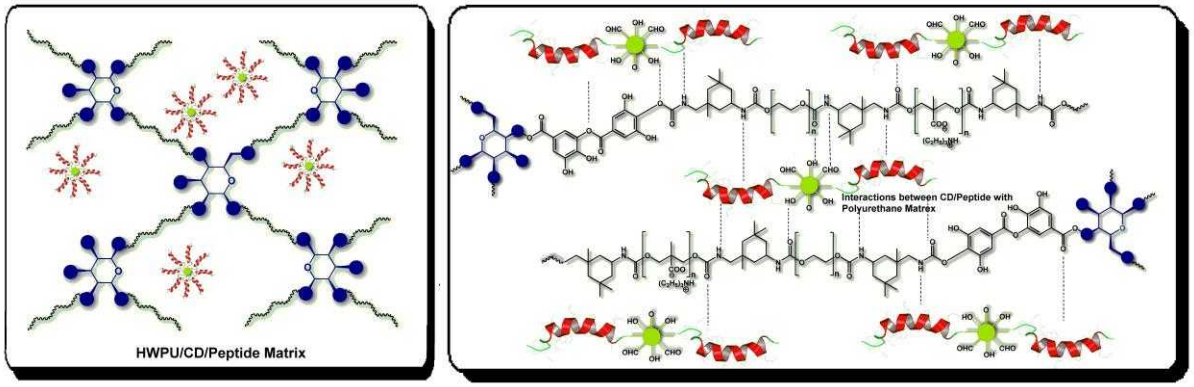

Scheme 2. WHPU/Gelatin/CD/Peptide Matrix (multifunctional PU) and plausible interaction between CD/peptide and WHPU matrix.

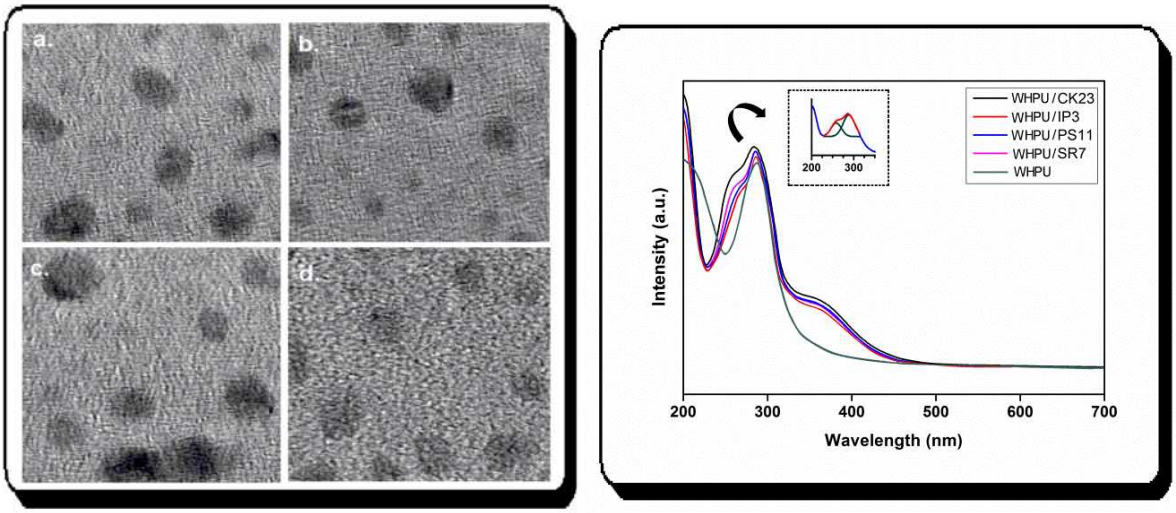

Figure 6. TEM image of **a.** WHPU/CK23, **b.** WHPU/IP3, **c.** WHPU/PS11, **d.** WHPU/SR7 and their UV-visible spectra.

Ex situ technique was employed to fabricate WHPU. Briefly, IPDI (4.44 g), PEG 600 (2.68 g) and BMPA (1.68 g) were reacted at 80-90 °C for 2 h keeping –NCO to –OH ratio is 1.5. In the next step, BD (0.90 g) and TA (1.24 g) were introduced at room temperature using THF as solvent. Reaction was carried out at 65-70 °C for another 5 h until no free –NCO group was detected by FTIR spectroscope. All the steps were carried out under the inert atmosphere of nitrogen with constant mechanical agitation. Finally, at a very slow rate water was added. THF was removed under reduced pressure. Conjugated CD/peptide (1 wt% of total solid content) was added to this aqueous solution of PU and mixed well by stirring. A 3D scaffold

with desired shape was prepared by pouring the above system with 10% of gelatin into a mold. Scaffold was dried by freeze drying process and used for different experiments. Graphical representation of the polymeric scaffold is shown in **Scheme 2.** TEM images of WHPU/CD/peptide matrix confirmed a uniform sharing of the bio-nanohybrid in the scaffold which is shown in **Figure 6**. Further, UV-visible spectroscopy confirmed the incorporation of CD/peptide conjugate in the polymer matrix.

3.5. Cytocompatibility of Carbon Dot

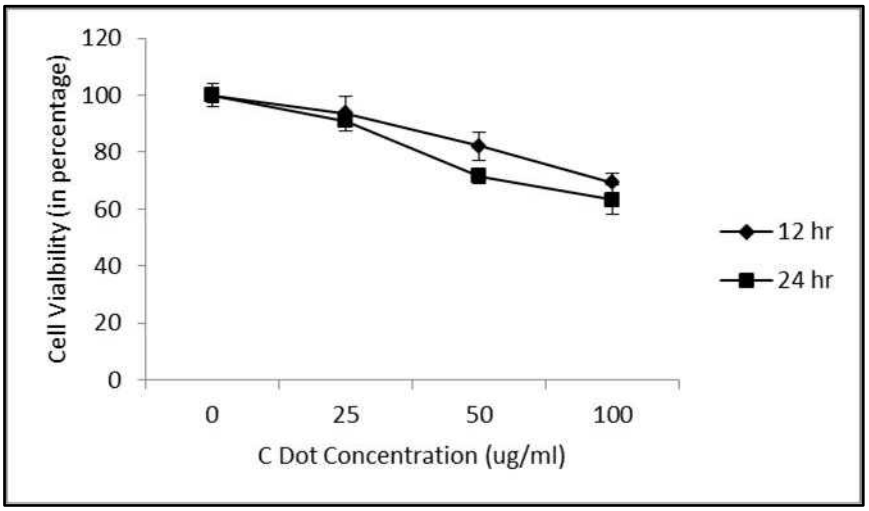

Figure 7. Cell viability assay against CD.

We have checked the cytocompatibility of CD on MG63 (human osteosarcoma cells) cell line by using MTT assay. The cells were incubated with different concentration of CD for two different time periods (12 h and 48 h). The graphical results shows that even at a higher concentration of CD (100ug/mL) the viability of the cells are above 60% for both the time periods. Moreover, the viability of MG63 cells at 12 h time period is greater than 80 per cent which gives us a preliminary confirmation that the CD is biocompatible with MG63 cells.

3.6. Biochemical characterization of developed peptide conjugated multifunctional hyperbranched polymer system

3.6.1. Cytotoxicity study

The bar graph in **Figure 8. A** shows the MG63 viability in percentage against the polymers and control. The waterborne polyurethane alone shows a low cell viability of 25% as compared

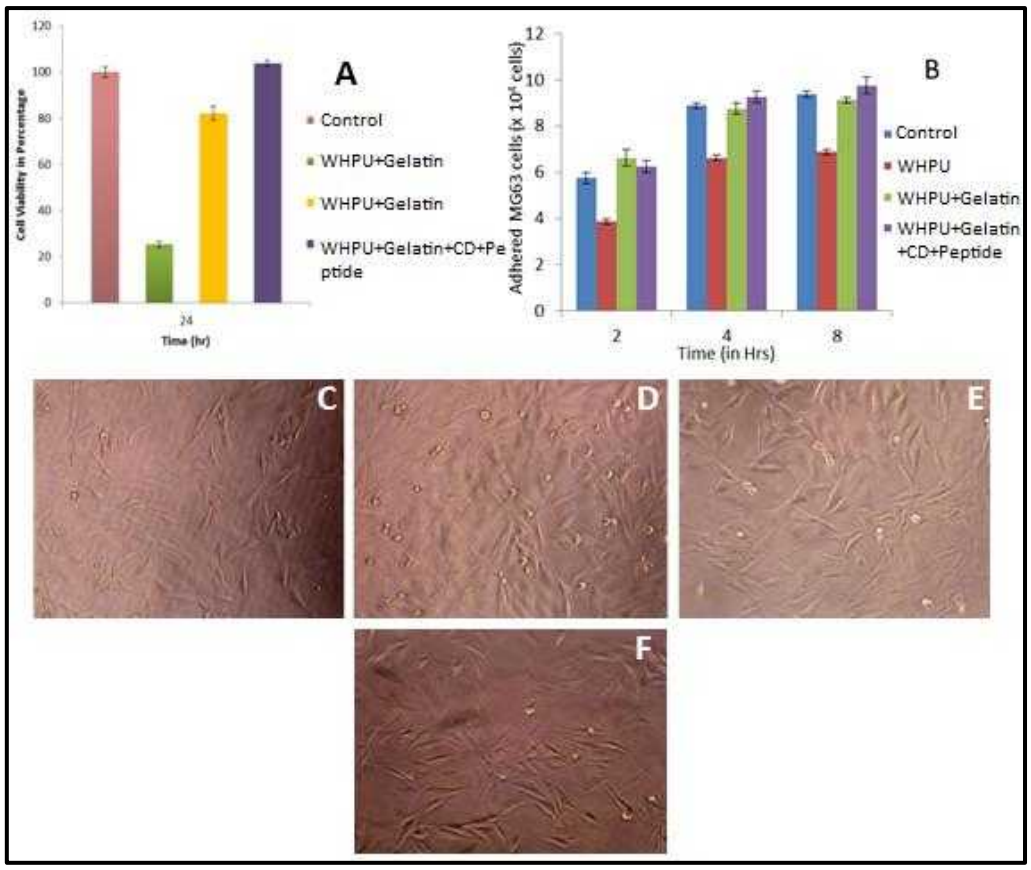

Figure 8. A. Cell viability assay of developed multifunctional hyperbranched dendritic polymer as analyzed by MTT assay, **(B)** Number of MG63 cells adhered plotted against time (hours) on control, WHPU, WHPU+Gelatin and Multifunctional PU. Bright Field images of MG63 cells adhered after 8 h on **(C)** Control, **(D)** WHPU, **(E)** WHPU+Gelatin , **(F)** WHPU+Gelatin+CD+Ppetide.

to control (cell viability 100% considered). After blending the polymer with gelatin, the compatibility of the polymer with MG63 cells has increased to near 80%. The cytocompatibility of the polymer increased to near 105% and is more compatible than the control, when peptide conjugated were added to the above WHPU-gelatin polymer.

3.6.2. Cell adhesion study

For MG63 the threshold adhesion time reached at 4th hour for all the cases. The degree of adhesion was compared, which differ for different material. According to the bar graph (**Figure 8.B**), with an initial seeding of 1 x 10^4 cells, the control (without polymer coating) shows an adherence of 90% (9 X 10^4 cells) after 4 h. Comparatively cells adherence seeded on WHPU polymer coated wells varied from 65% to 70% after 4 h and 8 h respectively. The

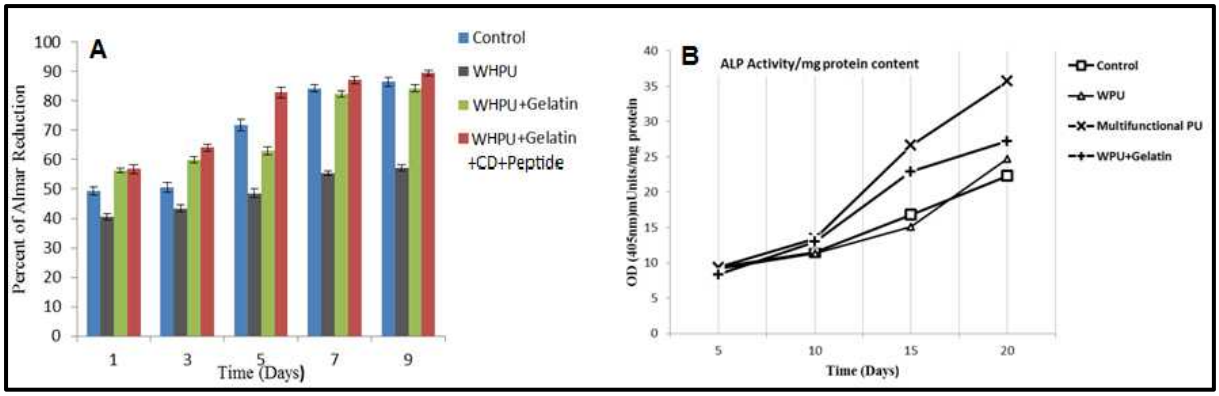

Figure 9. (A) Cell Proliferation assay of MG63 cells on different materials, **(B)** Cell differentiation of MG63 cells on different polymeric material was investigated by Alkaline Phosphatase Assay (ALP).

results of cell adhesion increased to 85-90% when WHPU polymer is blended with biopolymer gelatin, and almost 95% of cell adherence reached when seeded on WHPU+Gelatin+CD+Peptide (multifunctional PU) coated wells. The increment of cell adherence on hyperbranched multifunctional polyurethane material is due to the presence of adhesion peptide which has RGD sequence.

3.6.3. Cell Proliferation study

The *in vitro* proliferation of osteoblast was carried out by alamar blue assay and the proliferation rate was calculated as the percent of alamar reduction (**Figure 9. A**). Result shows at the end of day 7, that multifunctional PU's percent of alamar reduction is beyond 90% and even more than the control. WHPU shows lowest proliferation rate among all three (55% after day 7), and upon blending with gelatin the proliferation of MG63 increased to 80%. Clearly the result indicates that the biopolymer gelatin has a tremendous effect on the cell proliferation rate, which enhances with functionalization of the polymer with multiple peptides.

3.6.4. Cell Differentiation study

For differentiation study, *in vitro* alkaline phosphatase enzyme activity (ALP) of MG63 cells was checked (**Figure 9. B**). It was carried out to study the long term effect of multifunctional hyperbranched polymer on osteoblast differentiation. Osteoblast cells (10^4 cells) were cultured on polymer coated well and on non-coated well (as control). The supernatant of

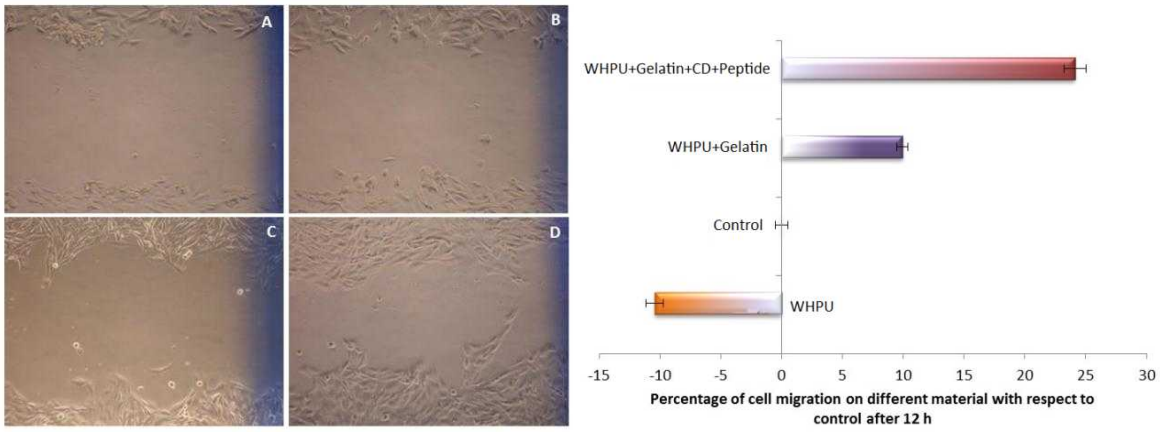

Figure 10. Adhered MG63 cells on plate were scratched to form a cell free zone at 0^{th} h **(A)** of control plate and **(B)** multifunctional PU coated plate. Cell migration observed after 12 h **(C)** of control plate **(D)** multifunctional PU coated plate. **(E)** Percentage of cell migration on different polymeric material coated plate with respect to control after 12 h.

the cell culture plate was collected at regular intervals (day 5^{th}, 10^{th}, 15^{th} and 20^{th}) and used for the analysis for the osteoblast differentiation. The procedure and calculation was done according to the manufacturer's instruction. The result shows that there is an increase in ALP activity on all the samples from day 10^{th} onwards. The highest ALP activity was found for the cells treated with multifunctional PU at day 20^{th}, which is 35 mU/mg protein, while the control and other treated cells shows activity varied from 20 mU to 25 mU per mg of protein. The study indicates that on prolonged exposure with the developed multifunctional polymer the osteoblast cell shows a sign of differentiation which is almost 1.5 times faster than the control. To further verify this hypothesis there is a need to check other markers such as the calcium content of the cell.

3.6.5. Osteoblast migration study

The rate of cell migration under the effect of polymeric materials was evaluated by scratch assay (**Figure 10**). With a 200 µL tip a scratch was made on the surface of the adhered cell. Image was taken at 0^{th} h after the scratch and another at 12^{th} h. The calculation for the rate of migration was done by Image J software. The graph shows the relative migration of MG63 cells on different material with relative to control. The rate of migration is fastest in multifunctional hyperbranched polyurethane with 24 times faster cell migration than control followed by gelatin blended WHPU. On the other hand, MG63 cell migration on

polymer WHPU is the slowest, and is 10 times slower than the control. Obviously, the adhesion peptides and presence of RGD sequence in gelatin has a profound effect on the cell adhesion and its migration.

3.7. RT-PCR based study on chronological state of the cell

Table 5. Primer sequences used for PCR based osteogenic gene fragment amplification

Gene	Primer Type	Primer Sequence	Amplicon
Glyceraldehyde 3 phosphate dehydrogenase	Forward	AGGTCGGTGTGAACGGATTTG	123
	Reverse	TGTAGACCATGTAGTTGAGGTCA	
Alkaline Phosphatase	Forward	CCAACTCTTTTGTGCCAGAGA	110
	Reverse	GGCTACATTGGTGTTGAGCTTTT	
Osteocalcin	Forward	GCAATAAGGTAGTGAACAGACTCC	101
	Reverse	AGCAGGGTTAAGCTCACACTG	
Collagen IA	Forward	CTGGCTTTGCCGGCC	77
	Reverse	ACCTTTAACACCAGTATCACCAGGT	

Study of osteoblast response towards the multifunctional polymer was carried out *in vitro* by RT-PCR study. MG63 cells were incubated with the multifunctional polymer for 5 and 10 days and the equal quantity of RNA from each sample was subjected to reaction to get complementary DNA, which then amplified by using gene specific PCR reaction. PCR reactions were set using four sets of gene specific primers (**Table 5**) targeted for assay of

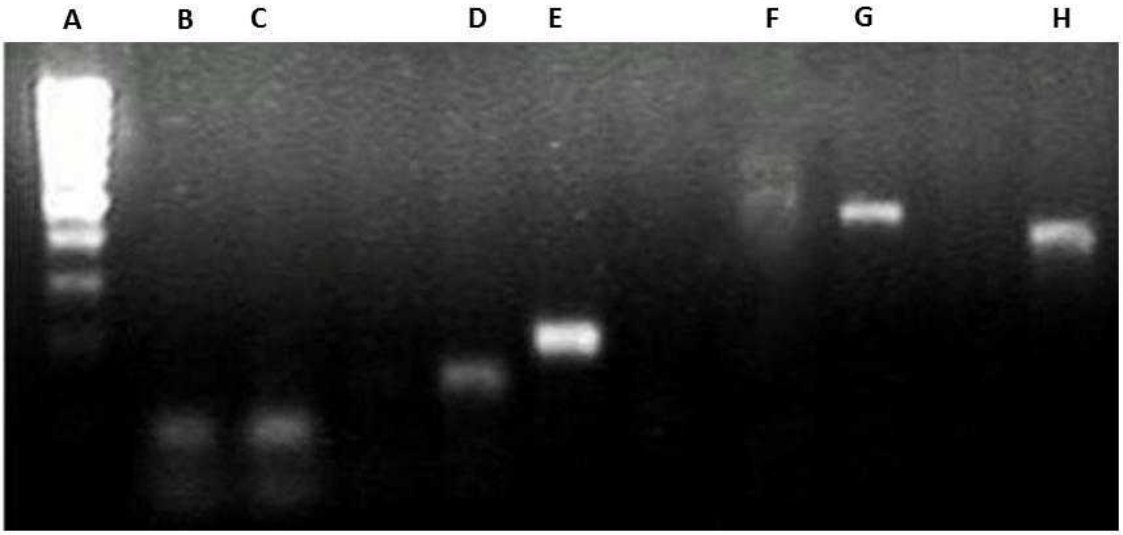

Figure 11. A. DNA marker, **B.** collagen IA (5 days), **C.** collagen IA (10 days), **D.** ALP (5 days), **E.** ALP (10 days), **F.** osteocalcin (5 days), **G.** osteocalcin (10 days), **H.** GAPDH

expression of RunX2, alkaline phosphatase, osteocalcin, collagen IA along with a house keeping gene, glyceraldehyde-3-phosphate dehydrogenase (GAPDH). The PCR products were verified via agarose gel electrophoresis. Data shows that the cells in 5 days incubation with polymer express collagen IA, alkaline phosphatase and osteocalcin in less quantity. The expression of alkaline phosphatase and osteocalcin increased on day 10^{th} cell extract, proves the fact that polymer is helping the cells to differentiate and induces mineralization. The collagen IA expression intensity at day 10^{th} remains same as that of day 5^{th}, which indicates that the polymer doesn't affect the cells in its rate of collagen IA production which is a major component of bone extracellular matrix.

3.8. In vivo study of multifunctional hyperbranched polymer as a non-invasive delivery vehicle

3.8.1. Murine osteoblast isolation and its characterization

Murine osteoblast was isolated by enzymatic digestion of calvariae of neonatal mice. Briefly, four neonatal mice, 3-4 days old, were euthanized via chloroform over anesthesia. The pubs were surface sterilized by submerging them in 70% ethanol for few minutes. Calvaria portion of the skull containing parietal and frontal bone pairs were dissected out and collected in cold DPBS in a sterile environment. The separated calvariae were chopped into

pieces of approximately 1 mm^2 and were digested enzymatically using 0.3% trypsin and 0.4% collagenase for 15 min at 37 °C with continuous agitation. The cells obtained out of

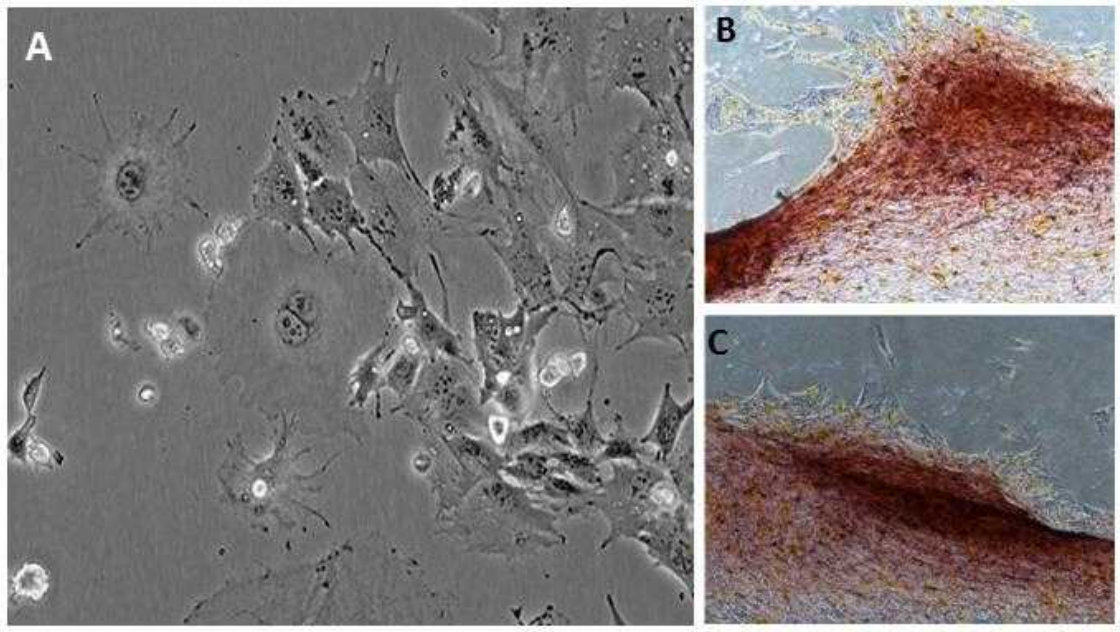

Figure 12. (A) Morphology of isolated murine osteoblasts cells viewed under microscope (magnification – 10X). **(B & C)** Cells were characterized for mineralization by staining with Alizarin red S solution.

each digestion were collected in complete medium. The digestate of third to fifth digestion were pooled together, filtered via 70 µm cell stainer and centrifuged at 250 g to obtain a cell pellet. The cell pellet thus obtained, was resuspended in complete α- MEM supplemented with 4 mM L-glutamine, 25 mM HEPES, 100 µM ascorbate-2-phosphate, 50 µg/mL gentamycin sulfate and 10% FBS. The cell suspension was seeded in a T-25 culture flask and cultured in an incubator at 37 °C incubator with 5% CO_2 with frequent change of media. Characterization of primary osteoblast obtained from the enzymatic digestion of murine calveria was done by mineralization study. The cells were seeded on a well, fixed and treated with Alizarin red S solution and incubated at 37 °C for 30 min. The wells were washed with PBS two three times after the incubation and stained cells were visualized under microscope. The osteoblast morphology was shown after first passage in **Figure 12**. The cells shows significant Alizarin red S staining after 5 days of culture, which indicates that the isolated cells are indeed bone cells and is not contaminated by other type of cells.

3.8.2. Ectopic bone formation study

Ectopic bone formation study was conducted to access the *in vivo* osteogenic capability of the developed peptide conjugated multifunctional dendritic polymer which was implanted

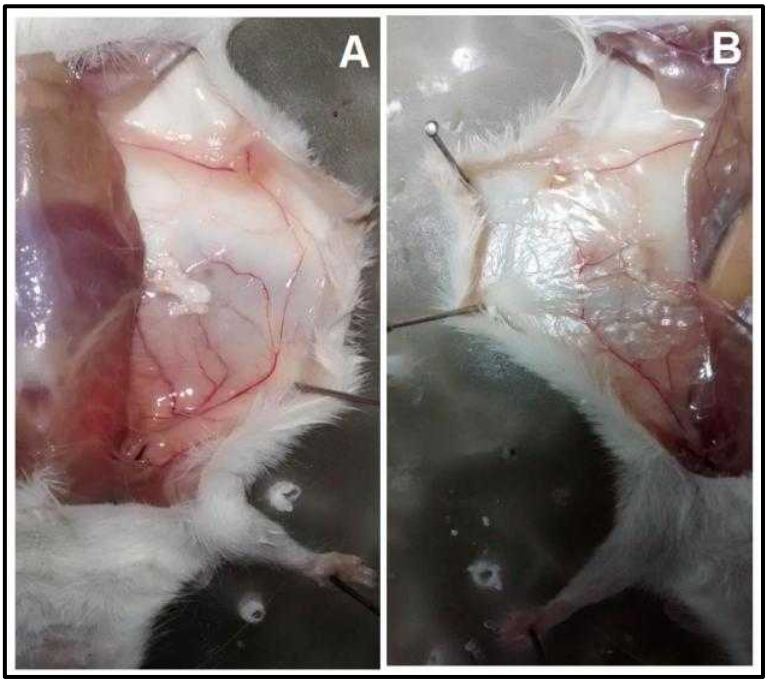

Figure 13. Representative macroscopic image of post-mortal mouse showing the location and texture of **(A)** Multifunctional PU and **(B)** WHPU with gelatin after 10 days of post implantation.

non-invasively in different inbreed mice (**Figure 13**). For the study, three variants of the selected polymeric gel formulations were considered for *in vivo* injection consisting of WHPU and Gelatin (without OB); WHPU, CD, peptides and Gelatine (without OB); WHPU, CD, Gelatin and peptides (with unaggregated OB). Briefly, 0.3 mL each of the three variants were aseptically injected subcutaneously via 16 gauge needles in different inbred mice near the dorsal region. In addition, each type of injection was made in two animals. The animals were maintained for 2 weeks with ample quantity of food and water. After the period, the animals were sacrificed and the injectates were retrieved for analysis.

3.8.3. Histochemistry

The retrieved injectate were fixed using neutral buffered formalin for 48 h with continuous agitation, followed by profuse washing in tap water. The samples were further

dehydrated using graded alcohols and the completely dehydrated samples were embedded in molten paraffin. The paraffins were cooled to room temperature and trimmed to partially expose the samples. The trimmed paraffin blocks were mounted on a rotary microtome (RM1215, Leica, Germany) and thin slices (5 µm) were cut from the samples. The

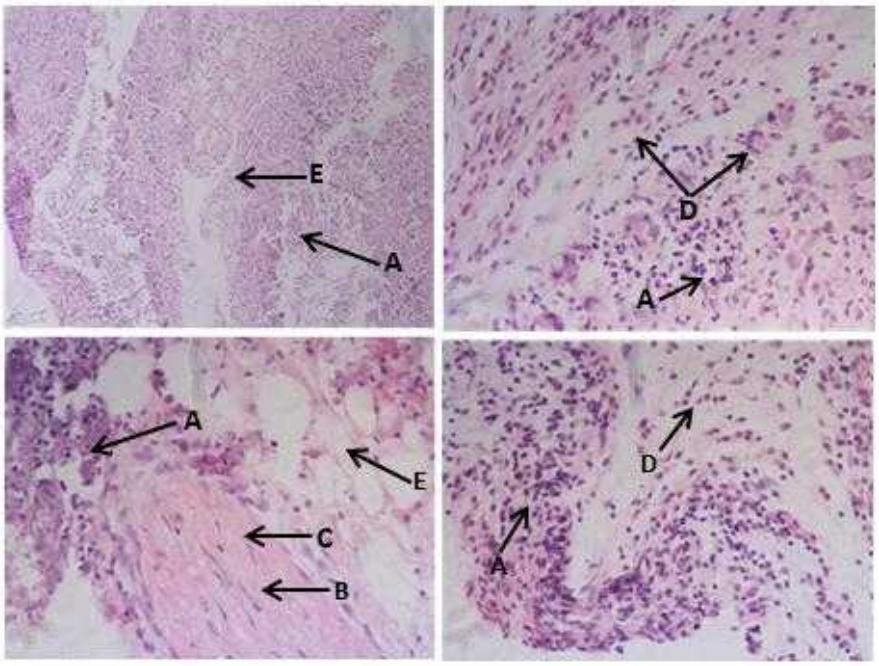

Figure 14. Representative histological section of the extracted explant viewed under the microscope after H & E staining. A=Osteoblast, B=Osteocytes, C=Mineralized area, D=Vascular tissue, E=Fat cell.

slices were mounted over APTES coated glass slides with the help of a tissue floatation bath. The slices were dewaxed and rehydrated using xylene and graded alcohols, respectively. To ensure a firm bonding between the tissue slices and glass surface, the slides were treated with warm Bouin's fluid for 15 min. The slides were then stained with Masson's trichrome stain (Sigma-Aldrich, USA) following the manufacturer's instructions. After staining the glass slides were dehydrated through graded alcohols and glass coverslips were mounted on the tissue slices using DPX mountant. The tissue sections were analysed under microscope the next day. The derived histological section with H&E staining shows normal morphological appearance and cellular organization (**Figure 14**). Larger part of the explant was covered by osteoblasts indicates the fact that the injectable polymer is osteogenic in nature and helps in its growth and proliferation even in an ectopic region. Few areas of the

explant shows mineralized area, with embedded osteocytes. This definitely confirms the differentiation and mineralizing capability of osteoblasts in vicinity of the polymer. Along with this vascular cell organization indicates vascularization capability of the injectate.

3.8.4. Mineralization study

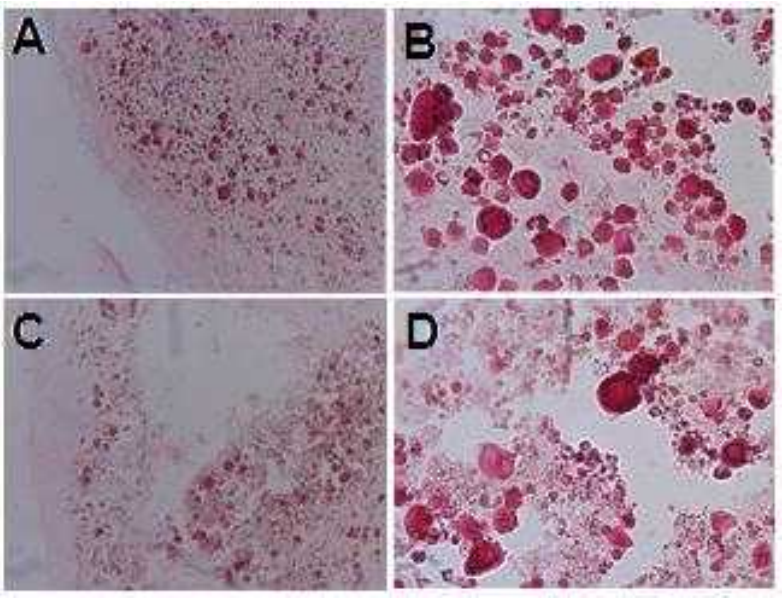

Figure 15. Section of the extracted explant was stained with Alizarin red S. Deposits of calcium is appeared red. Images of explant form inject ate multifunctional PU (A) 10X (B) 40X and from injectate WHPU with Gelatin.

The histological glass slides prepared from the method described previously, were used for the study of mineralization on the explant retrieved. In order to visualize mineralization nodules the glass slides were stained with Alizarin red S. Briefly, the fixed cells were exposed to a staining solution containing 1mg/mL of Alizarin red S (HiMedia) in distilled water the pH was adjusted to 5.5 with dilute ammonium hydroxide. After 15 min the staining solution was thoroughly washed with distilled water followed by imaging under a microscope (Scutt *et al.*, 2003). The result shows formation of multiple red spots throughout the tissue section indicates calcium deposition on the explant (**Figure 15**). The fact that mineralization occur in an ectopic region proves that the multifunctional polymer is very osteogenic in nature.

3.8.5. Confocal based vascularization study

Confocal microscopy imaging was performed to observe the vascularization pattern in the harvested explants. The explants fixed in histological slides were subjected to

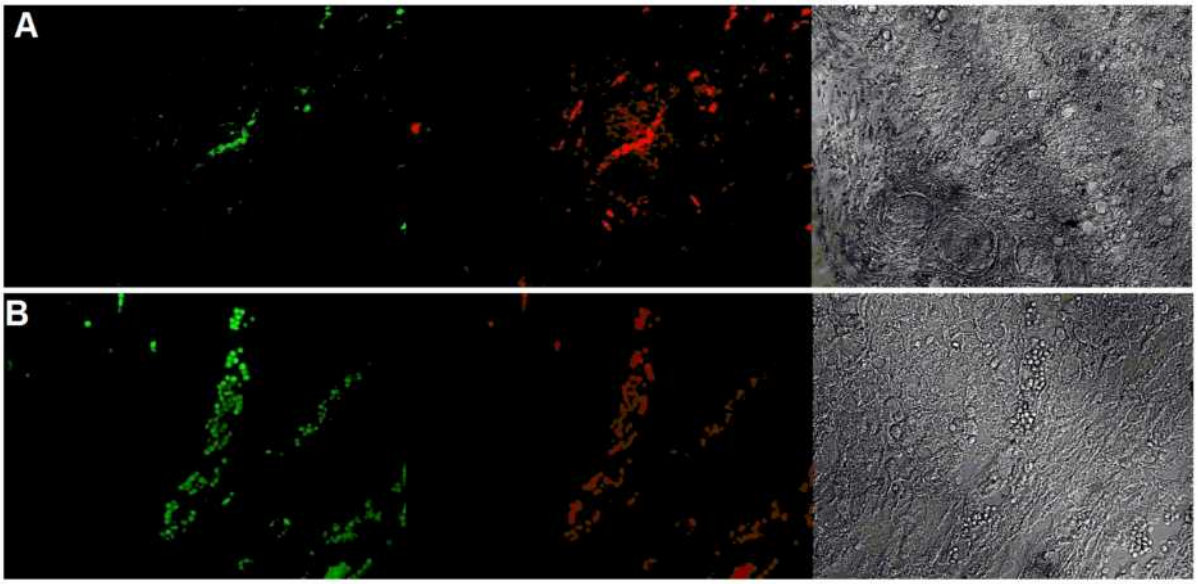

Figure 16. Whole mount confocal microscopy of the explant containing multifunctional PU as injectate. The freshly harvested explant shows a FITC (green) labeled anti-CD31 marking blood vessel lined endothelial cells. Red color shows the phalloidin stained cells. **(A)** 10X **(B)** 40X.

immunestaining with Phalloidin-Alexa Flour 594 (Abcam), FITC labeled anti-CD 31 monoclonal antibody (Abcam). The immunostained samples were sufficiently washed with TBS before confocal microscopy (Olympus FV1000, Japan). The micrographs (**Figure 16**) reveal the formation of vessel in the explant. The red dots stains phalloidin which indicates the presence of osteoblasts along with endothelial cells. The vessels were seen directed towards the patch of osteoblasts cells which indicates the occurrence of vascularization.

3.9. Biodegradation analysis

The degradation study was carried out with collagenase enzyme. Collagenase specifically cleaves collagen/gelatin fibrils at Gly775–Leu/Ile776, located in the region with a loose triple helical conformation. From the results, significant variation in the degradation profile of WPU, WPU+gelatin and peptide conjugated WPU+gelatin was observed. Among the three polymers, WPU+gelatin shows the maximum rate of degradation, where almost two-third of the polymer get degraded after 24 days. Relatively multifunctional hyperbranched polymer percentage of degradation rate is slower (~60%) and WPU shows the slowest percentage of

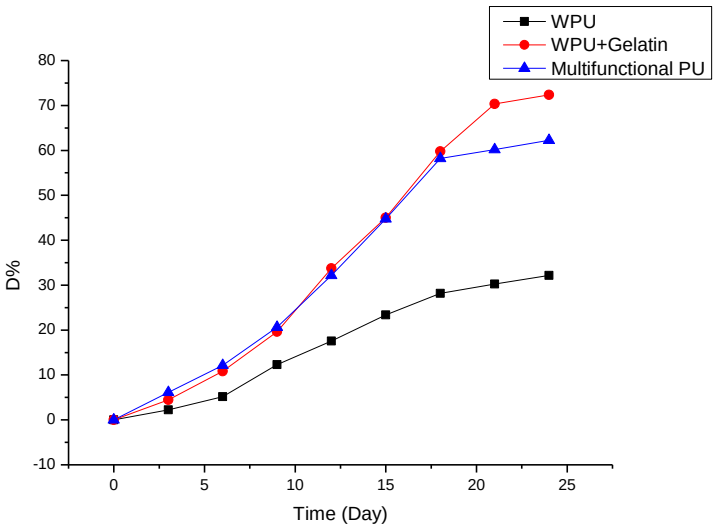

Figure 17. Degradation percentage of different hyperbranched dendritic polymer against collagenase.

degradation rate of 44% at the end of the analysis. The higher percentage of degradation rate of WPU+gelatin is might be due to the presence of biopolymer gelatin, which is a known substrate of collagenase enzyme. In the absence of biopolymer (WPU), the degradation rate changed drastically. The degradation rate of multifunctional hyperbranched polymer is comparatively slower, due to the physical interaction between peptide conjugated carbon dot and gelatin, which may prevent the exposure of collagenase specific cleavage site of gelatin, thus reducing the degradation rate. This reduced rate of polymer degradation would assist in proper bone wound healing.

References

1. Suh, J. K. F., & Matthew, H. W. (2000). Application of chitosan-based polysaccharide biomaterials in cartilage tissue engineering: a review. *Biomaterials*, *21*(24), 2589-2598.
2. Hubbell, J. A. (1995). Biomaterials in tissue engineering. *Nature Biotechnology*, *13*(6), 565-576.
3. O'Keefe, R. J., & Mao, J. (2011). Bone tissue engineering and regeneration: from discovery to the clinic—an overview. *Tissue Engineering Part B: Reviews*, *17*(6), 389-392.

4. Bruder, S. P., & Fox, B. S. (1999). Tissue Engineering of Bone: Cell Based Strategies. *Clinical orthopaedics and related research*, *367*, S68-S83.
5. Kühl, S., et al (2015). Detection of peri-implant bone defects with different radiographic techniques–a human cadaver study. *Clinical oral implants research*.
6. Hamann, C.' et al (2013). Sclerostin antibody treatment improves bone mass, bone strength, and bone defect regeneration in rats with type 2 diabetes mellitus. *Journal of Bone and Mineral Research*, *28*(3), 627-638.
7. Karak, N et al (2015). Bio-functionalized MWCNT/hyperbranched polyurethane bionanocomposite for bone regeneration. *Biomedical Materials*, *10*(2), 025011.
8. Bose, S., et al (2012). Recent advances in bone tissue engineering scaffolds. *Trends in biotechnology*, *30*(10), 546-554.
9. Pooyan, P., et al (2013). Design of a cellulose-based nanocomposite as a potential polymeric scaffold in tissue engineering. *Polymer*, *54*(8), 2105-2114.
10. Lakshmanan, R., et al (2013). Polymeric scaffold aided stem cell therapeutics for cardiac muscle repair and regeneration. *Macromolecular bioscience*, *13*(9), 1119-1134.
11. Rezwan, K., et al (2006). Biodegradable and bioactive porous polymer/inorganic composite scaffolds for bone tissue engineering. *Biomaterials*, *27*(18), 3413-3431.
12. Mistry, A. S., & Mikos, A. G. (2005). Tissue engineering strategies for bone regeneration. In *Regenerative Medicine II* (pp. 1-22). Springer Berlin Heidelberg.
13. Holmes, T. C. (2002). Novel peptide-based biomaterial scaffolds for tissue engineering. *TRENDS in Biotechnology*, *20*(1), 16-21.
14. Shin, H., et al (2003). Biomimetic materials for tissue engineering. *Biomaterials*, *24*(24), 4353-4364.
15. Burdick, J. A., & Anseth, K. S. (2002). Photoencapsulation of osteoblasts in injectable RGD-modified PEG hydrogels for bone tissue engineering. *Biomaterials*, *23*(22), 4315-4323.
16. Lutolf, M. P., & Hubbell, J. A. (2005). Synthetic biomaterials as instructive extracellular microenvironments for morphogenesis in tissue engineering. *Nature biotechnology*, *23*(1), 47-55.
17. Stevens, M. M. (2008). Biomaterials for bone tissue engineering. *Materials today*, *11*(5), 18-25.

18. He, X., et al (2012). New method for coupling collagen on biodegradable polyurethane for biomedical application. *Journal of Applied Polymer Science*, *126*(S1), E354-E361.
19. Hahn, C., et al (2012). Hydroxyl-functional polyurethanes and polyesters: synthesis, properties and potential biomedical application. *Polymer International*, *61*(7), 1048-1060.
20. Wang, W., & Wang, C. (2012). Polyurethane for biomedical applications: A review of recent developments. *The Design and Manufacture of Medical Devices*, 115-151.
21. Guo, B., et al (2013). Biodegradable and electrically conducting polymers for biomedical applications. *Progress in polymer science*, *38*(9), 1263-1286.
22. Luong-Van, E., et al (2013). Review: Micro-and nanostructured surface engineering for biomedical applications. *Journal of Materials Research*, *28*(02), 165-174.
23. Stefanakis, D., et al (2014). Synthesis of fluorescent carbon dots by a microwave heating process: structural characterization and cell imaging applications. *Journal of Nanoparticle Research*, *16*(10), 1-10.
24. Gong, N., et al (2014). Microwave-Assisted Polyol Synthesis of Gadolinium-Doped Green Luminescent Carbon Dots as a Bimodal Nanoprobe. *Langmuir*, *30*(36), 10933-10939.
25. Du, F., et al (2014). Economical and green synthesis of bagasse-derived fluorescent carbon dots for biomedical applications. *Nanotechnology*, 25(31), 315702.

B 2. Summary and Conclusions

In our current study, we tried to establish a combined approach in bone tissue engineering. A combined approached means developing a hyperbranched polymer which will have a properties of ideal matrix material and all the chemical cues required for fostering cellular growth and differentiation. In this regard, we prepared a waterborne polyurethane based hyperbranched polymer using tannic acid as bio-based component. To impart multifunctional nature to the polymer we linked the hyperbranched polyurethane with covalently conjugated surface functionalized carbon dot-peptides. To further augment the biocompatibility of the developed multifunctional polymer, gelatin (animal sourced biopolymer) was blended. The results of *in vitro* biological characterization such as osteoblast cell adhesion, proliferation, migration and differentiation shows a tremendous biocompatibility of the developed multifunctional hyperbranched polyurethane (peptide conjugated) than the control and only hyperbranched polyurethane (WPU). With the excellent *in vitro* results encouraged the authors to continue the ectopic *in vivo* study with the developed multifunctional polymer. The mineralization and vascularization study showed a significant deposition of calcium and blood vessel formation of the retrieved explant. The treated rats did not elicit any immunogenic behaviour towards implanted multifunctional polymer up to 10 days of the test. Thus, we successfully developed a peptide-dendritic polymer construct which is multifunctional in nature and could be directly applied for engineering of bone tissue in future. However encouraging, the results obtained hereby from ectopic bone formation experiment may not be extrapolated to a real bone defect situation. In certain cases ectopic bone formation is reported to be temporary in nature. Hence, in order to ascertain our findings, efficacy of osteoblast micro-tissues in bone regeneration is needed to be essentially tested *in vivo* in a critical defect model.

B 3. Details of new lead

1. Tannic acid was used as a perfectly branched moiety for the synthesis of hyperbranched polyurethane for the first time.
2. Carbon dot was synthesized from corms of *Colocasia esculenta*.
3. Carbon dot was incorporated with various peptides for the first time.
4. Carbon dot/peptide bio-nanohybrid was used for the fabrication of waterborne hyperbranched polyurethane as a novel scaffold material for the first time.
5. Blending of gelatin to the hyperbranched polyurethane increases the biocompatibility by approximately 30%.
6. The novel peptides conjugated multifunctional waterborne hyperbranched polyurethane developed showed tremendous biocompatibility towards osteoblasts cell line both *in-vitro* and *in-vivo.*

B 4. Details of Publications & Patents, if any

1. Gogoi, S., & Karak, N. (2014). Biobased Biodegradable Waterborne Hyperbranched Polyurethane as an Ecofriendly Sustainable Material. *ACS Sustainable Chemistry & Engineering*, *2*(12), 2730-2738. (Attached with the report)
2. Gogoi, S., Maji, S., Maiti T. K., & Karak, N. Gelatin Modified Waterborne Hyperbranched Polyurethane Carbon Dot/Peptide Bionanocomposite for Bone Tissue Regeneration. (Under Review, Joint communication with IIT, Khg)
3. Gogoi, S., Barua, S., & Karak, N. (2014). Biodegradable and Thermostable Synthetic Hyperbranched Poly(Urethane-Urea)s as Advanced Surface Coating Materials. *Progress in Organic Coatings*, *77*(9), 1418-1427.
4. Gogoi, S., Barua, S., & Karak, N. (2015). Cross-Linking Kinetics of Hyperbranched Epoxy Cured Hyperbranched Polyurethane and Optimization of Reaction Conversion by Central Composite Design. *Chemical Engineering Science*, *127*, 230-238.
5. Gogoi, S., & Karak, N. (2015). Bio-Based High-Performance Waterborne Hyperbranched Polyurethane Thermoset. *Polymers for Advanced Technologies*, *26*(6), 589-596.
6. Gogoi, S., Kumar, M., Mandal, B. B., & Karak, N. (2015). High Performance Luminescent Thermosetting Waterborne Hyperbranched Polyurethane/Carbon Quantum Dot Nanocomposite with *in vitro* Cytocompatibility. *Composites Science and Technology*, *118*, 39-46. (Attached with the report)

SECTION C

DETAILS OF GRANT UTILIZATION

Details of Assets acquired

Name of the Sanctioning Authority:		Department of Biotechnology (DBT)
1.	Sl. No.	106
2.	Name of the Grantee Institution	Tezpur University
3.	No. & Date of sanction order	BT/235/NE/TBP/2011, Dated April 30, 2012
4.	Amount of the sanctioned grant	Total=64.22 lakhs(Equipment=28.62 lakhs)
5.	Brief purpose of the grant	To develop multifunctional dendritic polymer system for bone tissue engineering
4.	Whether any condition regarding the right of ownership of Govt. in the Property or other assets acquired out of the grant was incorporated in the grant-in-aid sanction order.	No
*7.	Particulars of assets actually credited	PerkinElmer DSC-6000 with crimper and pan kit,TGA-4000 instrument and LVC sealer accessory kit with LVC Capsules.
8.	Value of the assets as on 30th April,2014	Total=Rs. 27,34,666.00 [USD 42000 (DSC & TGA), Rs. 2,21,750.00 (Accessories) Rs. 2,08,275.00 (LVCsealer accessory kit)]
9.	Purpose for which utilised at present	For thermogravimetric analysis and curing kinetics study
10.	Encumbered or not	Not
11.	Reasons, if encumbered	
12.	Disposed of or not	Not
13.	Reasons and authority, if any, for Disposal	NA
14.	Amount realised on disposal	NIL

Equipment	Unit price (US$)	Quantity	Total price (US$)
TGA-4000 instrument	17,405.00	1	17,405.00
DSC-6000 instrument	24,195.00	1	24,195.00
		Sub total	41,600.00
		Freight/ Handling	300.00
		Insurance	100.00
		Total	42,000.00

Accessories	Unit price (₹.)	Quantity	Total price (₹.)
Computer (Lenovo Thinkcenter)	45,000.00	2	90,000.00
HP Desktop Printer-109 G	5,000.00	2	10,000.00
Nitrogen gas cylinder & regulator (UHP Grade)	35,000.00	2	70,000.00
Oxygen gas cylinder & regulator (UHP Grade)	35,000.00	1	35,000.00
		Sub total	2,05,000.00
		CST	16,750.00
		Total	2,21,750.00

LVC sealer accessory kit	Unit price (₹.)	Quantity	Total price (₹.)
LVC sealer accessory kit	1,23,900.00	1	1,23,900.00
LVC St. St. Capsules	11,600.00	5	58,000.00
		Sub total	1,81,900.00
		CST	26,375.00
		Total	2.08,275.00

Utilization Certificate

(For the financial year ending 1st April, 2014 to 31st March, 2015)

(₹ in Lakhs)

1.	Title of the Project/Scheme:	**Development of Multifunctional Dendritic Polymers for Injectable Bone Tissue Engineering**
2.	Name of the Organization:	**Tezpur University**
3.	Principal Investigator:	**Professor Niranjan Karak**
4.	Deptt. of Biotechnology sanction order No. & date of sanctioning the project:	**BT/235/NE/TBP/2011 dated April 30, 2012**
5.	Amount brought forward from the previous financial year (2013-14) quoting DBT letter No. & date in which the the authority to carry forward said amount was given:	₹ **9.65027 lakhs**
6.	Amount received from DBT during the financial year (2014-15) (*please give No. and dates of sanction orders showing the amounts paid)*:	₹ **2.03 lakhs**
7.	Other receipts/interest earned, if any,	₹**1.27334 (From unspent amount of NRH)**
8.	Total amount that was available for expenditure during the financial year (1st April, 2014 to 31st March, 2015):	₹ **12.95361lakhs**
9.	Actual expenditure (excluding commitments) incurred during 1st April, 2014 to 31st March, 2015 (statement of expenditure is enclosed):	₹ **7.97627 lakhs**
10.	Unspent balance refunded, if any *(Please give details of cheque No. etc.):*	**NIL**
11.	Balance amount available at the end of 31st March, 2015:	₹ **4.97734 lakhs**
12.	Amount allowed to be carried forward to the next financial year (2014-15)vide letter No. & date:	**NA**

1. Certified that the amount of ₹ **7.97627 lakhs** mentioned against col. 9 has been utilised on the project/scheme for the purpose for which it was sanctioned and that the balance of ₹ **4.97734 lakhs** remaining unutilized at the end 31st March,

2015 will be adjusted towards the grants-in-aid payable during the next year (2015-16).

2. Certified that I have satisfied myself that the conditions on which the grants-in-aid was sanctioned have been duly fulfilled/are being fulfilled and that I have exercised the following checks to see that the money was actually utilised for the purpose for which it was sanctioned.

Kinds of checks exercised:

1. Cash Book

2. Ledgers

3. Vouchers

4. Bank statements

5. Annual accounts will be audited by C & AG in due course.

Statement of Expenditure referred to in para 9 of the Utilization Certificate

Showing grants received the Department of Biotechnology and the expenditure incurred during the period from 1st April, 2014 to 31st March, 2015.

(₹ in lakhs)

Items	Unspent balance carried for-Ward from previous year (2013-14) ₹	Grants received from DBT during the year (2014-15) ₹	Other receipts/interest earned, if any, on the DBT grants‡ ₹	Total of Col.(2+3+4)	Expenditure (excluding commitments) incurred during 1st April, 2014 to 31st March, 2015 ₹	Balance (5-6) ₹	Remarks ₹
1	2	3	4	5	6	7	8
1.Non-Recurring*							
Equipments	NIL	NIL	NIL	NIL	NIL	NIL	
2.Recurring							
i. Human resource	1.50806	0.44000	NIL	1.94806	1.46000	0.48806	
ii. Consumables	7.75558	1.59000	0.25000	9.59558	5.60480	3.99078	
iii. Travel	0.01068	NIL	0.40000	0.41068	0.21634	0.19434	
Iv. Contingency	0.28838	NIL	0.21334	0.50172	0.22820	0.27352	
v. Overhead	0.08757	NIL	0.41000	0.49757	0.46693	0.03064	
Total	9.65027	2.03000	1.27334	12.95361	7.97627	4.97734	

Manpower Staffing Details (For 1st April, 2014 to 31st March, 2015)

NAME OF THE PERSON	NAME OF THE POST	DATE OF JOINING	DATE OF LEAVING	TOTAL MONTHLY SALARY	TOTAL SALARY PAID DURING THE FINANCIAL YEAR (₹)	TOTAL SALARY PAID DURING PROJECT PERIOD (₹)
Satyabrat Gogoi	JRF	16th July, 2012	NA	12,000.00 upto July, 2014; 14,000.00 From August, 2014	1,46,000.00	3,92,194.00

Manpower Expenditure Details (For 1st April, 2014 to 31st March, 2015):

SANCTIONED POSTS	NUMBER	SCALE OF PAY	ANNUAL OUTLAY	OUTLAY FOR THE ENTIRE PERIOD	REVISED SCALE, IF ANY	REVISED ANNUAL OUTLAY	REVISED PROJECT OUTLAY	ACTUAL RELASES BY DBT	ACTUAL EXPENDITURE	BALANCE
JRF	1	12,000.00/ 14,000.00/	1,68,000.00	2,09,000.00	NA	NA	NA	1,94,806.00	1,46,000.00	48,806.00

Due- Drawn Statement (For 1st April, 2014 to 31st March, 2015)

Name of the Project Staff	Month and Year	Due (₹)	Drawn (₹)	Difference (₹)
Satyabrat Gogoi	April, 2014	12,000.00	12,000.00	0
	May, 2014	12,000.00	12,000.00	0
	June, 2014	12,000.00	12,000.00	0
	July, 2014	12,000.00	12,000.00	0
	August, 2014	14,000.00	14,000.00	0
	September, 2014	14,000.00	14,000.00	0
	October, 2014	14,000.00	14,000.00	0
	November, 2014	14,000.00	14,000.00	0
	December, 2014	14,000.00	14,000.00	0
	January, 2015	14,000.00	14,000.00	0
	February, 2015	14,000.00	14,000.00	0
	March, 2015	14,000.00	14,000.00	0

Utilization Certificate

(For the financial year ending 1st April, 2015 to 15th July, 2015)

(₹ in Lakhs)

13.	Title of the Project/Scheme:	**Development of Multifunctional Dendritic Polymers for Injectable Bone Tissue Engineering**
14.	Name of the Organization:	**Tezpur University**
15.	Principal Investigator:	**Professor Niranjan Karak**
16.	Deptt. of Biotechnology sanction order No. & date of sanctioning the project:	**BT/235/NE/TBP/2011 dated April 30, 2012**
17.	Amount brought forward from the previous financial year (2014-15) quoting DBT letter No. & date in which carry forward the the authority to said amount was given:	₹ **4.97734 lakhs**
18.	Amount received from DBT during the financial year (2015-16) (*please give No. and dates of sanction orders showing the amounts paid)*:	**NIL**
19.	Other receipts/interest earned, if any, on the DBT grants:	**NA**
20.	Total amount that was available for expenditure during the financial year (1st April, 2015 to 15th July, 2015):	₹ **4.97734 lakhs**
21.	Actual expenditure (excluding commitments) incurred during 1st April, 2015 to 15th July, 2015 (statement of expenditure is enclosed):	₹ **4.97734 lakhs**
22.	Unspent balance refunded, if any *(Please give details of cheque No. etc.):*	**NIL**
23.	Balance amount available at the end of 15th July, 2015:	**NIL**
24.	Amount allowed to be carried forward to the next financial year (2014-15)vide letter No. & date:	**NA**

1. Certified that the amount of ₹ **4.97734 lakhs** mentioned against col. 9 has been utilised on the project/scheme for the purpose for which it was sanctioned.

2. Certified that I have satisfied myself that the conditions on which the grants-in-aid was sanctioned have been duly fulfilled/are being fulfilled and that I have

exercised the following checks to see that the money was actually utilised for the purpose for which it was sanctioned.

Kinds of checks exercised:

1. Cash Book

2. Ledgers

3. Vouchers

4. Bank statements

5. Annual accounts will be audited by C & AG in due course.

Statement of Expenditure

Showing grants received the Department of Biotechnology and the expenditure incurred during the period from 1st April, 2015 to 15th July, 2015.

(Rs. In lakhs)

Items	Unspent balance carried for-Ward from previous year (2014-15) ₹	Grants received from DBT during the year (2015-16) ₹	Other receipts/interest earned, if any, on the DBT grants ₹	Total of Col.(2+3+4)	Expenditure (excluding commitments) incurred during 1st April, 2015 to 15th July, 2015 ₹	Balance (5-6) ₹	Remarks ₹
1	2	3	4	5	6	7	8
1.Non-Recurring							
Equipments	NIL	NIL	NIL	NIL	NIL	NIL	
2.Recurring							
i. Human resource	0.48806	NIL	NIL	0.48806	0.48806	NIL	
ii. Consumables	3.99078	NIL	NIL	3.99078	4.00009	-0.00931	
iii. Travel	0.19434	NIL	NIL	0.19434	0.22332	-0.02898	
Iv. Contingency	0.27352	NIL	NIL	0.27352	0.26152	+0.01200	
v. Overhead	0.03064	NIL	NIL	0.03064	0.00435	+0.02629	
Total	4.97734	NIL	NIL	4.97734	4.97734	NIL	

Manpower Staffing Details (For 1st April, 2015 to 15th July, 2015)

NAME OF THE PERSON	NAME OF THE POST	DATE OF JOINING	DATE OF LEAVING	TOTAL MONTHLY SALARY	TOTAL SALARY PAID DURING THE FINANCIAL YEAR (₹)	TOTAL SALARY PAID DURING PROJECT PERIOD (₹)
Satyabrat Gogoi	JRF	16th July, 2012	NA	12,000.00 upto July, 2014; 14,000.00 From August, 2014	48,806.00	4.41,000.00

Manpower Expenditure Details (For 1st April, 2015 to 15th July, 2015):

SANCTIONED POSTS	NUMBER	SCALE OF PAY	ANNUAL OUTLAY	OUTLAY FOR THE ENTIRE PERIOD	REVISED SCALE, IF ANY	REVISED ANNUAL OUTLAY	REVISED PROJECT OUTLAY	ACTUAL RELASES BY DBT	ACTUAL EXPENDITURE	BALANCE
JRF	1	12,000.00/ 14,000.00/	1,68,000.00	2,09,000.00	NA	NA	NA	nil	48,806.00	NIL

Due-Drawn Statement (For 1st April, 2015 to 15th July, 2015)

Name of the Project Staff	Month and Year	Due (₹)	Drawn (₹)	Difference (₹)
Satyabrat Gogoi	April, 2015	14,000.00	14,000.00	0
	May, 2015	14,000.00	14,000.00	0
	June, 2015	14,000.00	6,806.00	-7,194.00
	July, 2015 (Up to July 15th)	7,000.00	0.00	-7,000.00

3 Years Statement of Expenditure

Head	**Grant Received**				**Expenditure**				**Total Grant**	**Total Expenditure**	**Balance**
	1st Year 1 2012-13 **(₹)**	2nd Year 2 2013-14 **(₹)**	2nd Year 3 (Amount from Recurring Head) **(₹)**	3rd Year 4 2014-15 **(₹)**	1st Year 5 2012-13 **(₹)**	2nd Year 6 2013-14 **(₹)**	3rd Year 7 2014-15 **(₹)**	4th Year 8 2015-16 (Up to 15th July, 2015) **(₹)**	**(₹)**	**(₹)**	**(₹)**
Non Recurring	28.62	NIL	NIL	NIL		27.34666 +1.27334 (Transferred to Recurring Head)	NIL	NIL	28.62000	28.62000	NIL
Recurring											
Human Resource	2.11000	1.86000	NIL	0.44000	1.02194	1.44000	1.46000	0.48806	4.41000	4.41000	NIL
consumable	8.00000	7.55000	0.25000	1.59000	7.79442	NIL	5.60480	4.00009	17.39000	17.39931	-0.00931
Travel	0.50000	NIL	0.40000	NIL	0.20432	0.28500	0.21634	0.22332	0.90000	0.92898	-0.02898
Contingency	0.50000	NIL	0.21334	NIL	0.16996	0.04166	0.22820	0.26152	0.71000	0.70134	+0.01200
Overhead	1.00000	NIL	0.41000	NIL	0.50000	0.41243	0.46693	0.00435	1.41000	1.38371	+0.02629
Total	40.73000	9.41000	1.27334	2.03000	9.69064	30.79909	7.97627	4.97734	53.44334	53.44334	NIL

APPENDIX

SELECTED PUBLISHED PAPERS

ACS Sustainable Chemistry & Engineering

Research Article

pubs.acs.org/journal/ascecg

Biobased Biodegradable Waterborne Hyperbranched Polyurethane as an Ecofriendly Sustainable Material

Satyabrat Gogoi[†] and Niranjan Karak*[,†]

Advanced Polymer and Nanomaterial Laboratory, Department of Chemical Sciences, Tezpur University, Napaam, Tezpur, 784028 Assam, India

ABSTRACT: Research thrust to address the problems confronting the use of conventional polymers like high volatile organic compound (VOC) content still remains a challenge. In this context, the authors report the synthesis of a sustainable and biodegradable waterborne hyperbranched polyurethane (WHPU) using polyphenolic tannic acid in lieu of vegetable oil as the biobased component. The chemical structure of WHPU was characterized by nuclear magnetic resonance and Fourier transform infrared spectroscopy. An UV−visible peak at the wavelength of 282 nm confirmed the presence of catechol moiety in WHPU. WHPU exhibited pronounced thermostability and desirable performance (tensile strength, 6.87 MPa; elongation at break, 315%; scratch hardness, 5.5 kg for 15 wt % tannic acid based WHPU). The radical scavenging and hemolytic assays of WHPU showed their potent antioxidant activity and cytocompatibility with the erythrocytes, respectively. Furthermore, WHPU exhibited bacterial degradation by *Pseudomonas aeruginosa*. Thus, the above results forward the synthesized WHPU as a potent ecofriendly and sustainable polymeric material by a simple approach that possesses a higher degree of sustainability over a purely petrochemical route.

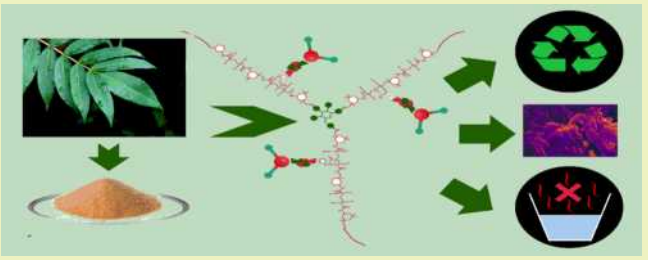

KEYWORDS: *Tannic acid, sustainable polymer, low VOC polyurethane, bacterial degradation, antioxidant*

INTRODUCTION

Since its inception, polyurethane has emerged as the material of interest in colossal domains owing to its versatile properties.[1,2] However, the growing consciousness regarding environmental issues has created serious concerns with respect to the use of conventional solvent borne polyurethanes, particularly due to high volatile organic compound (VOC) content.[3−5] The processing and application of solvent borne polyurethanes involve evaporation of organic solvents, which adds to VOC content in the atmosphere. Thus, different environment protection agencies have taken serious steps to reduce VOC emission from the industrial sector and issued guidelines to combat the same.[6] Under such circumstances, a paradigm shift in research has been observed in the develop ecofriendly polymeric materials. As a result of such efforts, waterborne polyurethane (WPU) has emerged out as one of the greener alternatives.[7] WPUs supersede their solvent borne counterparts in terms of nontoxicity, nonflammability, and low or no content of organic solvent.[8−11] Today, WPU has applications across the globe as a coating, adhesive, primer, paint additive, defoamer, associate thickener, pigment paste, biomaterial, etc.[12−14]

On the other hand, the global concern with respect to the dwindling petro-based resources and research according to tenets of green chemistry has instigated the utility of sustainable feedstock in the synthesis of industrially important polymers. Literature reports the use of various biobased raw materials including vegetable oils for the synthesis of WPU.[15−19] Madbouly et al. used castor oil for the synthesis of aqueous polyurethane dispersion.[4] Lu and Lorock synthesized WPU from soybean oil.[5] However, in such cases, oil needs to be transferred to the desired polyols, which increases the cost of the product. In this context, inexpensive, readily available biobased polyols may prove to be potent candidates for polyurethane synthesis. Thus, the present study intends to explore the potentiality of tannic acid, a readily abundant, low cost polyphenolic compound, as a bioderived raw material. The industrial viability of tannic acid has already been established in pharmaceutical and food industries and as a rust converter and mordant for dyeing.[20−22]

Further, literature cites use of hyperbranched polyester polyols for the synthesis of waterborne hyperbranched polyurethane (WHPU), a novel class of macromolecules with unique physical and chemical properties.[23−25] In this regard, the structure of tannic acid is interesting because of its architectural similarity with hyperbranched polyester polyols. Moreover, criteria of sustainability include environmental and health safety issues.[26,27] In this context, designing of tannic acid based hyperbranched polyurethane seems to be an interesting proposition because of significant bioactivity and biocompatibility.[28] Tannic acid can also act as a redox active material. Therefore, the potential interactions of tannic acid based WPU

Received: July 21, 2014
Revised: October 30, 2014

   dx.doi.org/10.1021/sc5006022 | ACS Sustainable Chem. Eng. XXXX, XXX, XXX−XXX

with biological systems need to be carefully examined to develop it as a safe and sustainable material.

The present study henceforth emphasizes the development of WHPU using tannic acid as a branch generating moiety, which is the first attempt in the field as per the author's knowledge. The study also made an effort to evaluate the hemocompatibility, radical scavenging activity, and biodegradability in order to highlight its potential as a safe and sustainable material.

EXPERIMENTAL SECTION

Materials. Isophorone diisocyanate (IPDI, Aldrich, Germany) and triethylamine (TEA, Merck, India) were used as received. Poly(ethylene glycol) with M_n = 600 (PEG-600, Merck, India); butane diol (BD, Merck, India), and tannic acid (TA, Sigma-Aldrich, Belgium) were dried in a vacuum oven at 55 °C prior to use. 2,2-Bis(hydroxymethyl)propionic acid (BMPA, Aldrich, Germany) was recrystallized from ethanol and dried before used. Tetrahydrofuran (THF, Merck, India) was distilled and stored in 4A molecular sieves for further use. Other chemicals like 1,1-diphenyl-2-picrylhydrazyl (DPPH), trichloroacetic acid and ferric chloride were purchased from Himedia, India and used as received. The bacterial strain of *Pseudomonas aeruginosa* (*P. aeruginosa*, MTCC 7814) was collected from the Department of Molecular Biology and Biotechnology, Tezpur University.

Synthesis of WHPU. WHPU was synthesized by a prepolymerization technique. Required amounts of IPDI, PEG-600, and BMPA (NCO/OH = 1.5) were taken in a four-necked round-bottomed flask equipped with a condenser, a nitrogen inlet, a thermometer, and a mechanical stirrer. The reaction was carried out at 80−90 °C for 2 h in nitrogen atmosphere with constant mechanical agitation. In the second step, BD and TA in THF were introduced to the reaction mixture at 25 °C, so that overall functional ratio of −NCO to −OH becomes 1 (considering three −OH groups of tannic acid participate in the reaction). Then the temperature was maintained at 65−70 °C for 5 h. After completion of the reaction, TEA was added slowly at room temperature in order to neutralize the −COOH groups under continuous stirring for 45 min. This was followed by slow addition of water to the reaction mixture with vigorous stirring for another 30 min. Then, THF was removed under reduced pressure in order to get the polymer in water. Three different compositions viz.WHPU05, WHPU10 and WHPU15 were prepared taking different weight percentages of TA (Table 1). Furthermore, control polyurethane (WPU0) without TA was also synthesized following the same method, except only BD was added in the second step in place of mixture of TA and BD. The synthesized polymers were cast on glass and a galvanized tin sheet to obtain a film thickness of 1−2 mm.

Table 1. Composition of the Reactants for the Synthesized Polyurethanes

composition	WPU0	WHPU05	WHPU10	WHPU15
IPDI (mol)	2.00	2.00	2.00	2.00
PEG 600 (mol)	0.80	0.80	0.80	0.80
BMPA (mol)	0.53	0.53	0.53	0.53
BD (mol)	0.67	0.60	0.54	0.50
TA (mol)	0	0.04	0.07	0.11
TEA (mol)	0.53	0.53	0.53	0.53
NCO/OH (functional ratio)	1.00	1.00	1.00	1.00

Characterization. Fourier transform infrared (FTIR) spectra were recorded on Nicolet (Madison, USA) FTIR Impact 410 spectrometer in absorbance mode using KBr pellets. The ^{1}H NMR spectrum was recorded on a 400 MHz FT NMR (Jeol, Japan) at 25 °C using trimethyl silane as the internal standard and D_2O as the solvent. UV spectra were recorded at room temperature (25 °C) using a Hitachi spectrophotometer (U2001, Tokyo, Japan). Thermal properties were evaluated by thermogravimetric analysis (TGA) and differential scanning calorimetry (DSC) study. Thermogravimetric study was carried out by using a PerkinElmer 4000 thermal instrument in the temperature range 25−700 °C, at a scanning rate of 10 °C/min, maintaining an inert atmosphere of nitrogen at a gas flow rate of 30 mL/min. The differential scanning calorimetry study was done by a PerkinElmer DSC 6000, USA instrument in the temperature range −70 to +120 °C (starting temperature = 0 °C) following a cycle of heating−cooling−heating under an atmosphere of nitrogen and at a scanning rate of 5 °C/min. Mechanical properties, such as tensile strength and elongation at break were measured by a Universal Testing Machine (UTM, Zwick Z010, Germany) equipped with a 5 kN load cell operated at a crosshead speed of 50 mm/min. Samples with dimensions 10 × 1 × 0.02 cm were used for the same. The scratch hardness of the polymeric films was measured by using a scratch hardness tester, Model No.705 (Sheen instrument limited, UK) with a stylus accessory at a travel speed of 30−40 mm/s. An Ubbelohde viscometer was used to determine the intrinsic viscosity of the synthesized polymers. Molecular weight of the polymer was determined by gel permeation chromatography (GPC, Waters, UK). On the other hand, images of the biodegraded polymer films were obtained by scanning electron microscopy (SEM, model JSM-6390LV (JEOL)), after platinum coating on the surface.

Radical Scavenging Assay. For DPPH radical scavenging assay, 1 mL of 0.1 M DPPH (in 50% ethanol solution) was mixed with 1 mL of polymer solution (0.2−2.0 mg/mL in double distilled water). The reaction mixture was vortexed and incubated at room temperature for 20 min under dark conditions. Then the absorbance was measured at 517 nm.[29] The scavenging activity was measured by using the following formula

$$\text{scavenging effect (\%)} = \left[1 - \frac{A_{S-517}}{A_{C-517}}\right] \times 100$$

where $A_{S\text{-}517}$ is the absorbance of the samples and $A_{C\text{-}517}$ is the absorbance of the control.

For hydroxyl radical scavenging assay, 1 mL of polymeric solution (0.2−2.0 mg/mL in double distilled water) was mixed with 2.4 mL of 0.1 M phosphate buffer (pH 7.4) and 0.6 mL of 0.4 M H_2O_2 solution. The mixture was vortexed and incubated for 10 min at room temperature. The absorbance was measured at 230 nm.[29] The scavenging ability for hydroxyl radicals was calculated by using the following formula

$$\text{scavenging effect (\%)} = \left[1 - \frac{A_{S-230}}{A_{C-230}}\right] \times 100$$

where $A_{S\text{-}230}$ is the absorbance of samples and $A_{C\text{-}230}$ is the absorbance of the control.

The reduction potential of WHPU was determined by mixing 1 mL of polymer solution (0.2−2.0 mg/mL in double distilled water) with 1 mL of 0.2 M phosphate buffer (pH 6.6), 0.5 mL of 1% (w/v) potassium ferricyanide. The mixture was incubated at 50 °C in a water bath for 20 min. Then it was cooled, followed by addition of 1 mL of 10% (w/v) trichloroacetic acid and 0.2 mL of 0.1% (w/v) freshly prepared ferric chloride solution. The resulting solution was shaken well and the absorbance was measured at 700 nm.[29] The reducing power was calculated by using the following formula

$$\text{reducing power} = A_{S-700} - A_{C-700}$$

where $A_{S\text{-}700}$ is the absorbance of the sample and $A_{C\text{-}700}$ is the absorbance of the control with replacement of $FeCl_3$ by water. For all the experiments, ascorbic acid (As) was taken as the standard to compare the radical scavenging activity of WHPU compositions.

Hemolytic Assay. To get preliminary knowledge about the cytocompatibility of WHPU, hemolytic assay was performed. The idea was to investigate lysis of the red blood cell (RBC) membrane by the tested macromolecule. Goat's blood collected in heparinized tube containing 4% sodium citrate was centrifuged for 20 min at 3000 rpm (503 g). The erythrocytes were washed thrice with phosphate buffer

dx.doi.org/10.1021/sc5006022 | ACS Sustainable Chem. Eng. XXXX, XXX, XXX−XXX

Scheme 1. Synthesis of WHPU

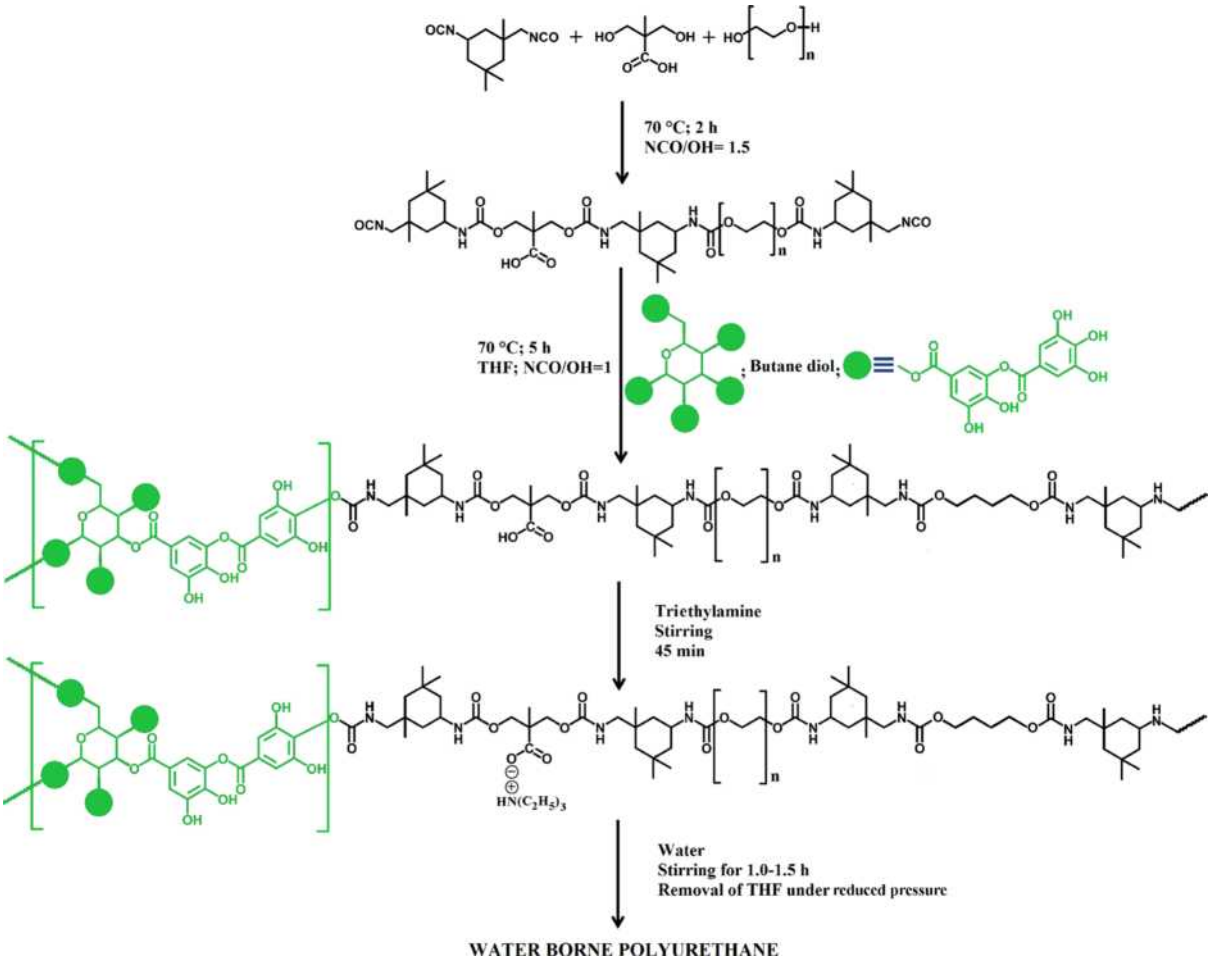

saline. Then 5% hematocrit was obtained by resuspending the packed erythrocytes in PBS (10 mM at pH of 7.4). Samples with varying concentrations viz. 0.25, 0.50, 0.75, 1.00, and 5.00 mg mL^{-1} were prepared. Then 100 mL of each sample was taken in a microfuge tube along with 1900 mL of the hematocrit and the solutions were incubated at 37 °C for 30 min. After completion of the incubation period, cells were placed in ice bath for 1 min followed by centrifugation at 3000 rpm (503 g) for 5 min. Then hemoglobin concentration was determined by the help of UV absorbance at 540 nm as a measure of hemolysis.[30] The experiment was performed in triplicate and analyzed by one way ANOVA.

Biodegradation Study. Biodegradation study was done by McFarland turbidity method using *P. aeruginosa* as the bacterial strain.[31,32] A medium of mineral salts containing 2.0 g of $(NH_4)_2SO_4$, 2.0 g of Na_2HPO_4, 4.75 g of KH_2PO_4, 1.2 g of $MgSO_4{\cdot}7H_2O$, 0.5 mg of $CaCl_2{\cdot}2H_2O$, 100 mg of $MnSO_4{\cdot}5H_2O$, 70 mg of $ZnSO_4{\cdot}7H_2O$, 10 mg of $H_3BO_3{\cdot}5H_2O$, 100 mg of $CuSO_4{\cdot}7H_2O$, 1 mg of $FeSO_4{\cdot}7H_2O$, and 10 mg of MoO_3, all in 1.0 L of demineralised water, was prepared. It was sterilized for 15 min at 120 °C under a pressure of 15 lb and then allowed to cool to room temperature. Bacterial strain of *P. aeruginosa* was cultured in the medium inside an incubator shaker at 37 °C for 48 h. 100 μL (10^8 microbes/mL, as calculated by McFarland turbidity method) of the cultured medium was taken in a conical flask containing 10 mL of the prepared salt medium. The polymeric films were sterilized by exposing them to UV light of wavelength 254 nm. The sterilized films were incubated inside the medium under sterile condition at 37 °C. Medium without polymeric films was used as the negative control. The increase in turbidity of the medium with time indicates bacterial growth. The optical density (OD) of the microorganism was monitored by measuring the absorbance of the medium at 600 nm with respect to the control. The experiment was conducted in triplicate for an experimental period of 6 weeks. FTIR analysis of the degraded films was also conducted to study the functional changes occurred due to bacterial degradation.

RESULTS AND DISCUSSION

Synthesis. Synthesis of WHPU involves use of low reactive aliphatic diisocyanate, a diol or diamine chain extender and a component with ionogenic center. In the present work, IPDI was used as the diisocyanate, PEG-600 and BD were used as the diol, and BMPA was used as the ion generating moiety. The literature demonstrates the use of hyperbranched polyester polyols for the synthesis of WHPU. The current work used TA as a biobased raw material for the same. TA is structurally very much similar to a hyperbranched polyester, with five branches generating from a pyranose heterocycle, 25 hydroxyl groups, and 10 ester linkages. Hence, the present synthesis tried to utilize TA instead of a synthetic polyester polyol to construct hyperbranched structure. In practice, all 25 hydroxyl groups of TA are not equally reactive because of steric reasons. This steric factor becomes more prominent when TA reacts with long and bulky prepolymer chains. Moreover, substitution of one hydroxyl group by a prepolymer chain frequently reduces the reactivity of others, present in the system. Hence, TA was used in a calculated amount that ensures participation of at least three hydroxyl groups in the urethane reaction. In relation to the solubility parameter, the unreacted and free −OH groups are crucial as they can enter into secondary interactions like hydrogen bonding with polar solvents causing enhanced

dx.doi.org/10.1021/sc5006022 | ACS Sustainable Chem. Eng. XXXX, XXX, XXX−XXX

solubility of the polymer. Further, in the first step of the synthesis, mainly $-NCO_{secondary}$ is expected to react, since in absence of catalyst $-NCO_{secondary}$ is known to have preferred selectivity toward urethane reaction (Scheme 1).[33] A maximum of 15 wt % of TA was used, as exceeding this amount can lead to an uncontrolled reaction and may cause gelation. Weight-average (M_w) and number-average (M_n) molecular weight; polydispersity index (PDI) and solution viscosity of synthesized polymers are given in Table 2. Weight-average molecular weight was obtained in the range of 22 600 to 25 700 with molecular distribution between 1.23 and 1.39 using THF as the solvent. The molecular weight was found to follow an increase in trend with the tannic acid content of the polymer.

Table 2. Weight Average (M_w), Number Average (M_n) Molecular Weight; Polydispersity Index (PDI) and Solution Viscosity of WHPUs

parameter	WHPU05	WHPU10	WHPU15
M_w (g/mol)	22600	23300	25700
M_n (g/mol)	16200	18900	21700
PDI	1.39	1.23	1.34
solution viscosity (dL/g)	0.365	0.298	0.274

FTIR Study. FTIR spectroscopy was used to confirm the variety of chemical functionalities present in the polymer matrix (Figure 1). Further, evidence of hydrogen bonding was also gathered by following the change in frequency and intensity of the peaks in the mid-IR spectral region.[31] For the studied systems, the absorption band near 1720−1730 cm^{-1} can be attributed to −C═O stretching frequency (contribution from both amide I and ester linkages). Further, the −N—H stretching and −N—H bending (amide II) frequenies were observed at 3410 and 1580 cm^{-1}, respectively. The absorption peak for C═C bond was near 1600 cm^{-1}. Similarly, amide III, which is mainly due to in-phase combination of N—H in plane bending and C—N stretching vibration occurred near 1230−1236 cm^{-1}. Amide IV and amide V bands were observed at frequencies of 773−776 and 631−635 cm^{-1}, respectively. On the other hand, a shift of IR band toward lower wavenumber was witnessed in the amide I and N—H stretching region with increase of TA content in the polymer. This indicates involvement of hydrogen bonding between phenolic −OH from TA and urethane −NH and −C═O groups. With increasing TA content, there will be more −OH groups in the polymer matrix by which the extent of hydrogen bonding gets strengthened.

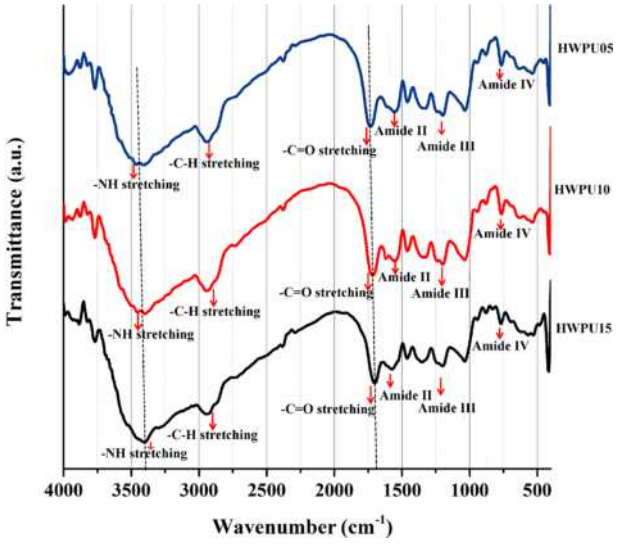

Figure 1. FTIR spectra of WHPU05, WHPU10, and WHPU15.

^{1}H NMR Study. The interpretation of ^{1}H NMR spectrum of the synthesized WHPU is difficult, as IPDI is composed of two isomeric forms (Z and E) and two isocyanate groups ($-NCO_{primary}$ and $-NCO_{secondary}$) that exhibit variable selectivity toward urethane reaction under different conditions.[33] Though, ^{1}H NMR data depicted in Figure 2 furnish valuable evidence in favor of the synthesized polymer. It is well understood from the mechanism of urethane reaction that in absence of any catalyst, $-NCO_{secondary}$ of IPDI has preferred selectivity toward urethane reaction. Hence, in the first step of synthesis, mostly $-NCO_{secondary}$ is expected to react with −OH functionality. The −N**H** urethane peaks were observed at δ 7.8−8.0 ppm, which confirmed the formation of two different urethanes viz. cis and trans. The appearance of surface functional phenolic protons (Ph−O**H**) was marked at δ 9.7−9.9 ppm. Aromatic protons belonging to TA were observed at δ 7.0−7.2 ppm. However, from the ^{1}H NMR spectrum, a quantitative calculation of degree of branching is difficult for IPDI/TA derived polyurethane, as the peaks of interest were very complex aggregates.

UV−Visible Spectroscopy. The catechol units of TA produce an absorbance peak near 280 nm, which can be used to detect and evaluate quantitative amount of TA present in the polymer. For the synthesized polymer, absorbance was observed near 282 nm in the UV−visible spectrum. The intensity of the peak for the catechol moiety increases with the increase of TA content, as depicted in Figure 3. This indicates the presence of more catechol units in the polymer with increase in wt % of TA.

Thermal Properties. Thermogravimetric analysis showed that WHPU exhibited a two-step thermal degradation pattern, as shown in Figure 4a. The first step (in the temperature range 250−260 °C) can be attributed to the degradation of thermolabile aliphatic moieties, urethane bonds, and ester groups, whereas the second step (in the temperature range 300−320 °C) is due to the degradation of aromatic rings belonging to TA moiety. It is clearly understood from the depicted thermograms that TA content in the polymer can enhance the thermal stability of WHPU, which is consistent with the wt % of TA in the polymers. Further, weight residue left after degradation up to 700 °C also increases with TA content. High thermostability of TA imparted by aromatic moieties, ester linkages, heterocyclic ring system, as well as enhanced secondary interactions like hydrogen bonding, contribute toward the thermal properties of WHPU. Better thermal behavior of WHPU compared to WPU0 further confirmed the fact. The glass transition temperature (T_g) measurement was made by using DSC at the heating rate of 5 °C/min in a nitrogen atmosphere for the temperature range of −70 to +200 °C. The DSC curves shown in Figure 4b indicate that T_g increases with increase in wt % of TA. This could be due to increase in inter- and intramolecular interactions in the structure.

Mechanical Properties. Mechanical properties were evaluated for the synthesized WHPUs. The different mechanical properties are documented in Table 3. The tensile strength and scratch hardness increase, and elongation at break

dx.doi.org/10.1021/sc5006022 | ACS Sustainable Chem. Eng. XXXX, XXX, XXX−XXX

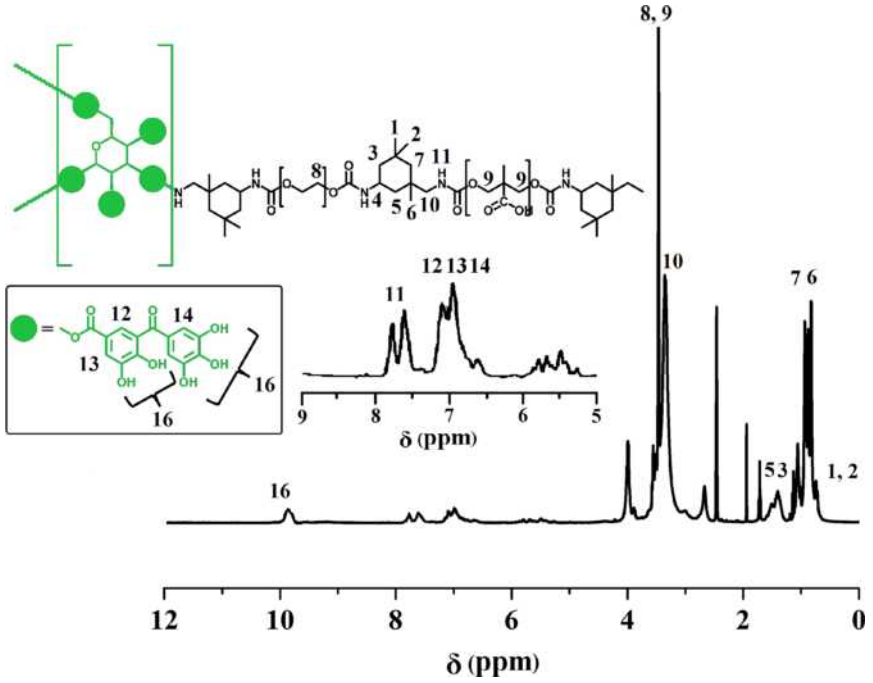

Figure 2. ^{1}H NMR spectrum of WHPU15.

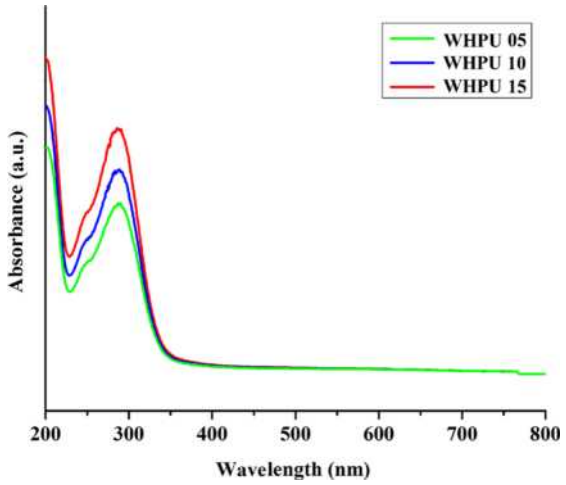

Figure 3. UV−visible spectra of WHPU05, WHPU10, and WHPU15.

decreases with increase in wt % of TA in WHPUs. Generally, mechanical properties depend on many factors viz. presence of polar groups within the polymeric chains, existence of inter and intramolecular interactions, entanglement of chains, compositions and nature of reactants, molecular weight, rigidity of the polymer, etc. Addition of TA can favor the above factors by virtue of its high molecular structure and rigidity. Moreover, different intermolecular interactions, e.g., polar−polar, hydrogen bonding between macromolecular chains get strengthened with the TA content. This results high strength of the polymer. However, TA content can affect the polymer chain flexibility due to molecular rigidity, which results in reduction of the elongation at the break values. However, all the polymers possess good bending and gloss values.

Radical Scavenging Assay. The antioxidant potency of a compound relies on its ability to donate labile electron to a radical. Radical scavenging assay of WHPU against DPPH and hydroxyl radical shows profound antioxidant activities (Figure 5a,b). It is obvious, because the polymer contains a large number of free catechol moieties. These catechol fractions can act as an electron donor that reacts with free radicals to convert them into more stable products with the termination of radical chain reactions. WHPU15 exhibits the best radical scavenging activity whereas WHPU05 shows the least. This is due to the greater tannic acid content of the former than the latter. The reducing power assay also reflects the overall antioxidant activity of a compound. It is based on reduction of Fe^{3+} to Fe^{2+} with change in color of the mixture from yellow to various shades of blue or green according to the reducing power of the sample. The results obtained are in accordance with the radical scavenging assay data (Figure 5c). Among tested polymers, WHPU15 exhibited a greater reducing power than WHPU10 and WHPU05 and, at higher concentrations, it is comparable with the reducing ability of ascorbic acid (As). WPU0 did not exhibit any radical scavenging activity, which confirms that TA is the vital component of the polymer responsible for antioxidant activity of WHPUs. This radical scavenging ability of the macromolecule is significant in multiple respects. The literature shows use of natural, antioxidant polyphenolic polymers in the control of glucose intolerance and diabetes.[34] Polymers with antioxidant activity have also been reported as a medium to suppress oxidative stress injury to the cells.[35] In this context, TA based synthetic WPU shows the promise as a potent sustainable material with profound bioactivity. Moreover, polyphenolic antioxidants have reportedly used to enhance thermo-oxidative stability of different polymeric materials.[36] Hence, the presence of the polyphenolic fraction within the same macromolecular structure adds the advantage of high thermo-oxidative stability to the developed polymer.

Hemolytic Assay. Human health safety is one of the major criteria for material sustainability. A material should not create any potential hazard to the living beings during its life cycle. Hence, in order to scrutinize material safety of the synthesized system, hemolytic assay was performed as a representative biocompatibility test. It is a type of acute toxicity assay used to

dx.doi.org/10.1021/sc5006022 | ACS Sustainable Chem. Eng. XXXX, XXX, XXX−XXX

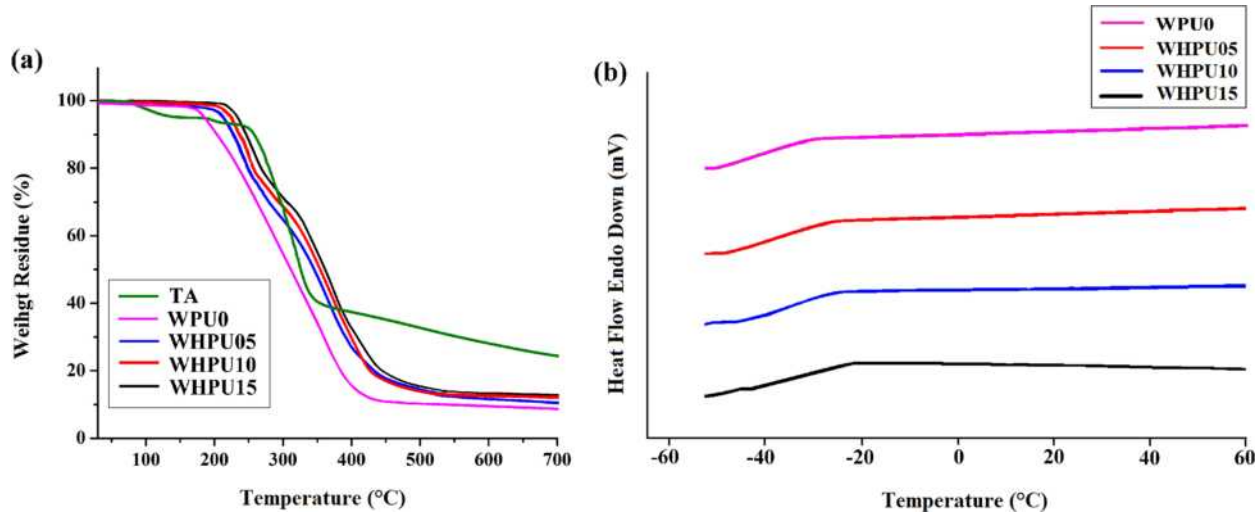

Figure 4. (a) TGA thermograms of WPU0, WHPU05, WHPU10, WHPU15, and TA. (b) Glass transition temperatures of WPU0, WHPU05, WHPU10, and WHPU15.

Table 3. Mechanical Properties of WHPUs

property	WHPU05	WHPU10	WHPU15
tensile strength (MPa)	4.93 ± 0.15	6.02 ± 0.20	6.87 ± 0.17
elongation at break (%)	508 ± 5	457 ± 7	315 ± 4
scratch hardness (kg)	4.0 ± 0.2	5.0 ± 0.1	5.5 ± 0.2
gloss (60 °C)	98.7 ± 0.7	94.5 ± 0.8	88.2 ± 0.4

evaluate the hemocompatibility of material by detecting hemolyzation of erythrocytes. Such study involves direct interaction of a material with the erythrocyte membrane in which the extent of disruption of the erythrocyte membrane is a direct measure of toxicity. The RBC hemolytic protection assay reveals that WHPU15, WHPU10, and WHPU05 were well compatible with the mammalian erythrocytes compared to WPU0 (Figure 6). WHPU15 exhibited the best compatibility among the tested WHPUs, though the differences are very minute. Twin 20, the negative control, showed high absorbance of hemoglobin, which indicated drastic rupture of the RBC membrane. Contrarily, the positive control (hematocrit) exhibited a negligible absorbance value. Thus, in vitro hemolytic assay confirmed the compatibility of the polymer with mammalian RBC.

Biodegradation Study. Biodegradation of WHPU by *P. aeruginosa* bacteria was studied by determining the weight loss

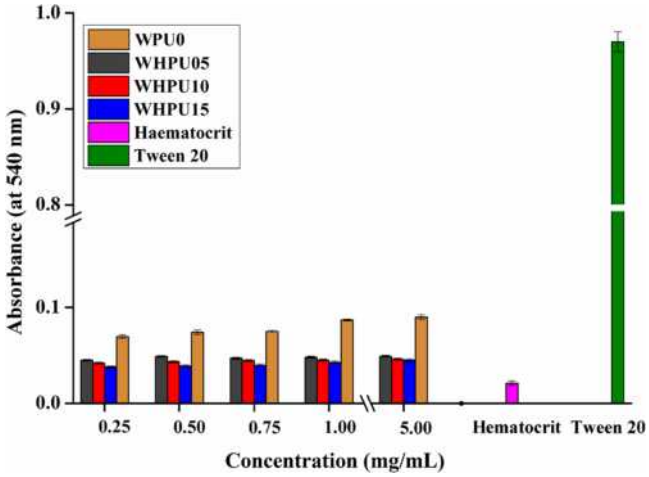

Figure 6. Antihemolytic activity assessment.

with time due to exposure of bacterial strain. The curve of retention of weight percentage versus incubation period depicted in Figure 7a clearly showed degradation of the polymeric films after 6 weeks of exposure. WHPU15 is found more biodegradable compared to WHPU10 and WHPU05. It is because of the fact that polyester polyurethanes are more

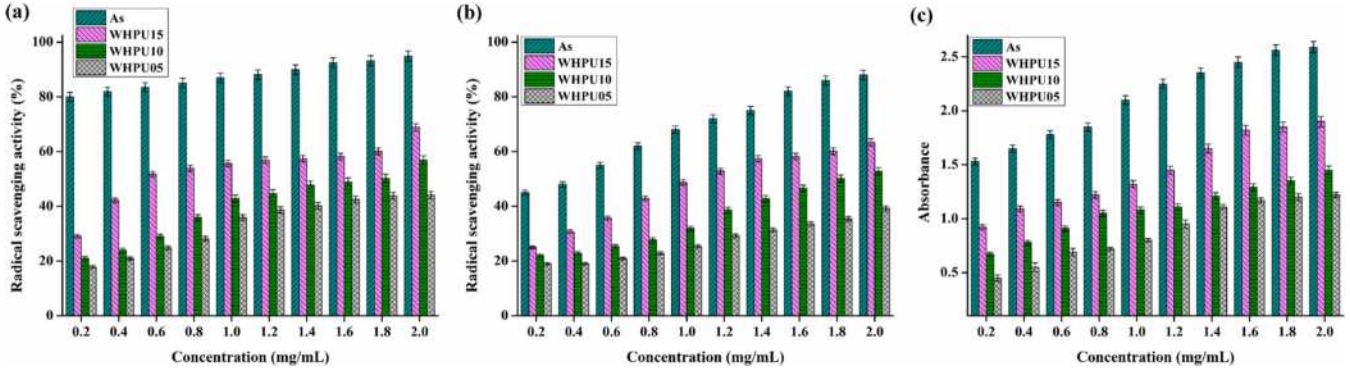

Figure 5. (a) DPPH radical scavenging activity, (b) hydroxyl radical scavenging activity, and (c) reducing power assay of WHPU05, WHPU10, and WHPU15.

dx.doi.org/10.1021/sc5006022 | ACS Sustainable Chem. Eng. XXXX, XXX, XXX−XXX

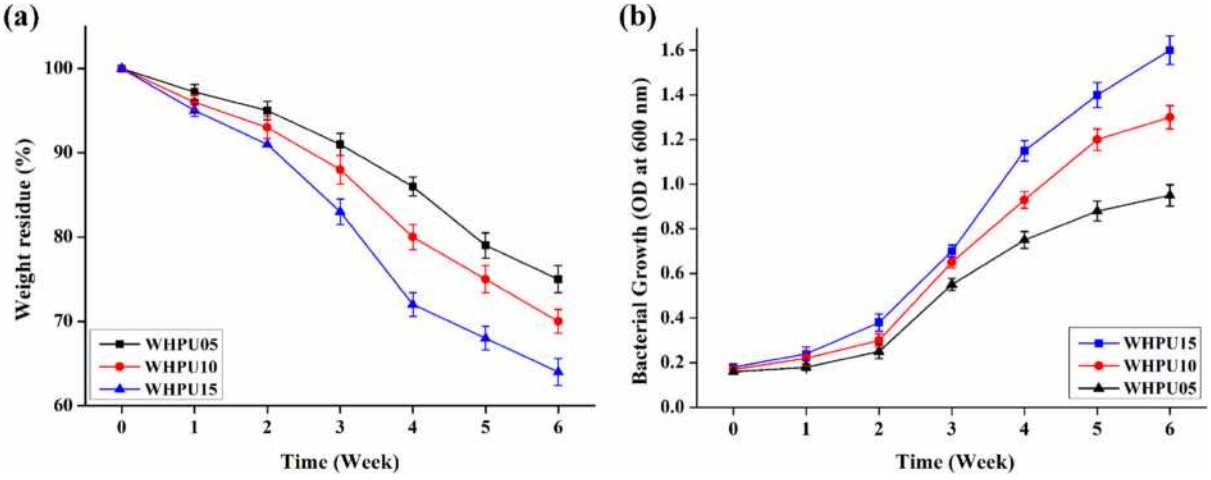

Figure 7. (a) Weight loss profile of WHPU05, WHPU10, and WHPU15 due to bacterial degradation. (b) Growth curve of *P. Aeruginosa* on WHPU05, WHPU10, and WHPU15.

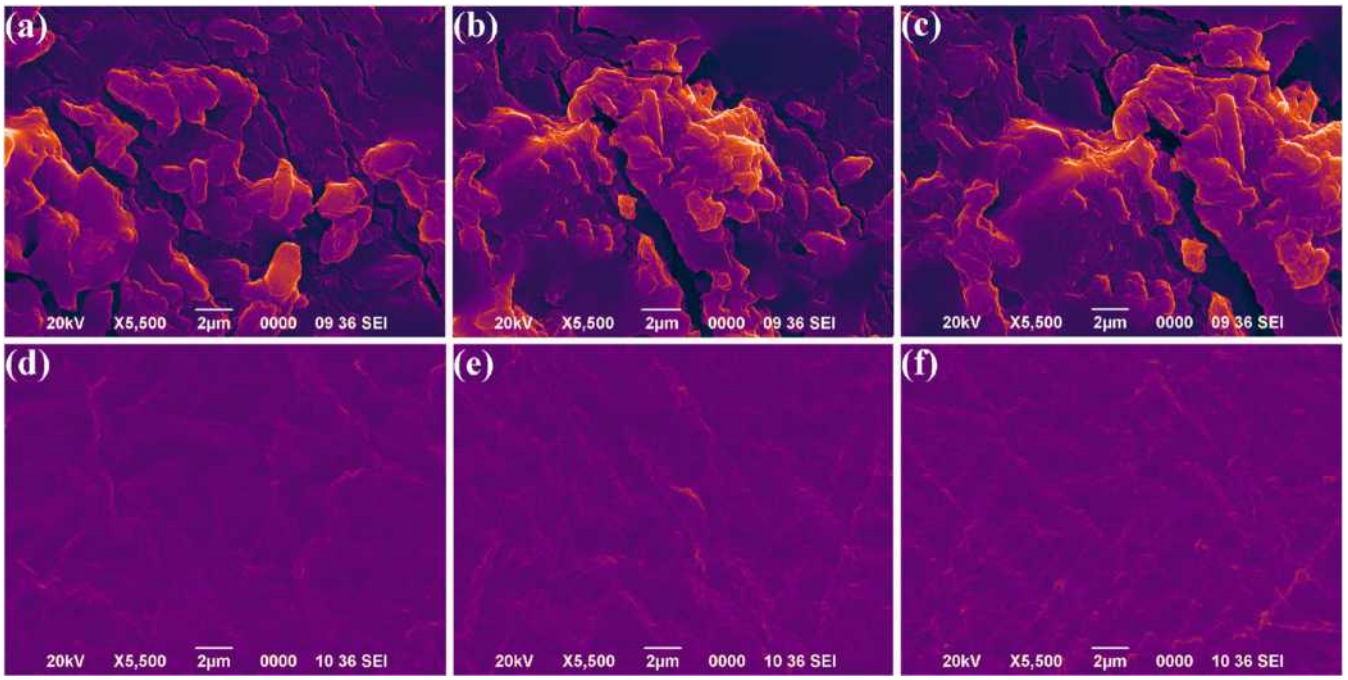

Figure 8. SEM images of biodegraded (a) WHPU05, (b) WHPU10, and (c) WHPU15, and respective controls of (d) WHPU05, (e) WHPU10, and (f) WHPU15.

susceptible toward microbial degradation compared to polyurethane alone.[37] As WHPU15 contains more hydrolyzable ester linkages, it offers a better liable surface for bacterial growth. This is further supported by the OD curves shown in Figure 7b. There is a linear increment in the bacterial population with time of incubation, which was found to follow an increasing trend with TA content in the polymer. WHPU05 contains less ester linkages, hence weight loss as well as bacterial growth is the least. The bacterial biodegradation was further confirmed by SEM images taken after 6 weeks of degradation (Figure 8). For all the polymer compositions, significant bacterial adherence and surface erosion was witnessed compared to the controls. Here it is pertinent to mention that WPU0 is also biodegradable, though within 10 days, no significant degradation was observed. FTIR study of the degraded film further confirmed the bacterial degradation as a number of significant changes have been observed in the spectra (Figure 9). The most distinct change was observed for the carbonyl stretching frequency (1720−1730 cm^{-1}) with significant diminution in peak intensity over the experimental period. On the other hand, the absorbance peaks resulting from urethane (−NH) and aryl groups remain unchanged. This primarily indicates that degradation is mainly occurred by the rupturing of the eater linkages.

CONCLUSIONS

The present study reported a more environmentally benign approach over the conventional petrochemical routes to synthesize a hyperbranched waterborne polyurethane using tannic acid as a biobased material. The polymer exhibited acceptable thermal and mechanical properties. Hence, it can be concluded that tannic acid and other biobased polyphenolic

dx.doi.org/10.1021/sc5006022 | ACS Sustainable Chem. Eng. XXXX, XXX, XXX−XXX

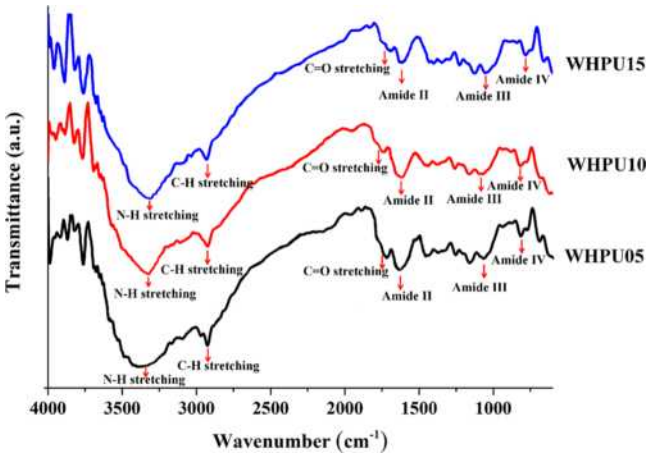

Figure 9. FTIR spectra of biodegraded WHPUs after 6 weeks of bacterial exposure.

compounds could be good alternative of vegetable oils for the development of sustainable polymeric materials. Furthermore, hemolytic assay confirmed the erythrocyte compatibility and radical scavenging assay revealed potent antioxidant activity of the polymer. These results indicate the polymer as a safe material. Biodegradability of the polymer by bacterial strain can address genuine problems of land pollution and solid waste management issues. The overall results mandate the synthesized waterborne hyperbranched polymer as a step toward sustainability.

AUTHOR INFORMATION

Corresponding Author

*N. Karak. E-mail: karakniranjan@yahoo.com. Tel: + 91-3712-267009. Fax: +91-3712-267006.

Author Contributions

†The paper was written through contributions of all authors. All authors have given approval to the final version of the paper. These authors contributed equally.

Funding

DBT, India, Grant No. BT/235/NE/TBP/2011, dated April 30, 2012; SAP (UGC), India, Grant No. F.3-30/2009 (SAP-II); FIST program-2009 (DST), India, Grant No. SR/FST/CSI-203/209/1, dated June 5, 2010.

Notes

The authors declare no competing financial interest.

ACKNOWLEDGMENTS

The authors thank Mr. Shaswat Barua for helping out in the study of bacterial biodegradation and hemolytic assay and Ms. Sujata Pramanik for her valuable suggestions during the work.

REFERENCES

(1) Zia, K. M.; Bhatti, H. N.; Ahmad, I. Methods for polyurethane and polyurethane composites, recycling and recovery: A review. *React. Funct. Polym.* **2007**, *67*, 675−692.

(2) Delebecq, E.; Pascault, J. P.; Boutevin, B.; Ganachaud, F. On the versatility of urethane/urea bonds: Reversibility, blocked isocyanate, and non-isocyanate polyurethane. *Chem. Rev.* **2012**, *113*, 80−118.

(3) Asif, A.; Shi, W. UV curable waterborne polyurethane acrylate dispersions based on hyperbranched aliphatic polyester: Effect of molecular structure on physical and thermal properties. *Polym. Adv. Technol.* **2004**, *15*, 669−675.

(4) Madbouly, S. A.; Xia, Y.; Kessler, M. R. Rheological behavior of environmentally friendly castor oil-based waterborne polyurethane dispersions. *Macromolecules* **2013**, *46*, 4606−4616.

(5) Lu, Y.; Larock, R. C. Soybean-oil-based waterborne polyurethane dispersions: Effects of polyol functionality and hard segment content on properties. *Biomacromolecules* **2008**, *9*, 3332−3340.

(6) Kim, B. K.; Kim, T. K.; Jeong, H. M. Aqueous dispersion of polyurethane anionomers from H_{12}MDI/IPDI, PCL, BD, and DMPA. *J. Appl. Polym. Sci.* **1994**, *53*, 371−378.

(7) Noble, K. L. Waterborne polyurethanes. *Prog. Org. Coat.* **1997**, *32*, 131−136.

(8) Kim, B. K.; Seo, J. W.; Jeong, H. M. Morphology and properties of waterborne polyurethane/clay nanocomposites. *Eur. Polym. J.* **2003**, *39*, 85−91.

(9) Kuan, H. C.; Ma, C. C. M.; Chang, W. P.; Yuen, S. M.; Wu, H. H.; Lee, T. M. Synthesis, thermal, mechanical and rheological properties of multiwall carbon nanotube/waterborne polyurethane nanocomposite. *Compos. Sci. Technol.* **2005**, *65*, 1703−1710.

(10) Seo, J. W.; Kim, B. K. Preparations and properties of waterborne polyurethane/nanosilica composites. *Polym. Bull.* **2005**, *54*, 123−128.

(11) Li, Y.; Noordover, B. A.; van Benthem, R. A.; Koning, C. E. Reactivity and regio-selectivity of renewable building blocks for the synthesis of water-dispersible polyurethane prepolymers. *ACS Sustainable Chem. Eng.* **2014**, *2*, 788−797.

(12) Gao, C.; Xu, X.; Ni, J.; Lin, W.; Zheng, Q. Effects of castor oil, glycol semi-ester, and polymer concentration on the properties of waterborne polyurethane dispersions. *Polym. Eng. Sci.* **2009**, *49*, 162−167.

(13) Liu, H. L.; Dai, S. A.; Fu, K. Y.; Hsu, S. H. Antibacterial properties of silver nanoparticles in three different sizes and their nanocomposites with a new waterborne polyurethane. *Int. J. Nanomed.* **2010**, *5*, 1017−1028.

(14) Rahman, M. M.; Kim, E. Y.; Yun Kwon, J.; Yoo, H. J.; Kim, H. D. Cross-linking reaction of waterborne polyurethane adhesives containing different amount of ionic groups with hexamethoxymethyl melamine. *Int. J. Adhes. Adhes.* **2008**, *28*, 47−54.

(15) Eissen, M.; Metzger, J. O.; Schmidt, E.; Schneidewind, U. 10 years after Rio—Concepts on the contribution of chemistry to a sustainable development. *Angew. Chem., Int. Ed.* **2002**, *41*, 414−436.

(16) Xia, Y.; Larock, R. C. Vegetable oil-based polymeric materials: Synthesis, properties, and applications. *Green Chem.* **2010**, *12*, 1893−1909.

(17) Meier, M. A.; Metzger, J. O.; Schubert, U. S. Plant oil renewable resources as green alternatives in polymer science. *Chem. Soc. Rev.* **2007**, *36*, 1788−1802.

(18) De, B.; Gupta, K.; Mandal, M.; Karak, N. Biodegradable hyperbranched epoxy from castor oil-based hyperbranched polyester polyol. *ACS Sustainable Chem. Eng.* **2013**, *2*, 445−453.

(19) Knight, S. C.; Schaller, C. P.; Tolman, W. B.; Hillmyer, M. A. Renewable carvone-based polyols for use in polyurethane thermosets. *RSC Adv.* **2013**, *3*, 20399−20404.

(20) Khan, N. S.; Ahmad, A.; Hadi, S. M. Anti-oxidant, pro-oxidant properties of tannic acid and its binding to DNA. *Chem.-Biol. Interact.* **2000**, *125*, 177−189.

(21) Burkinshaw, S. M.; Kumar, N. The mordant dyeing of wool using tannic acid and $FeSO_4$, Part 1: Initial findings. *Dyes Pigments* **2009**, *80*, 53−60.

(22) Singh, D. D. N.; Yadav, S. Role of tannic acid based rust converter on formation of passive film on zinc rich coating exposed in simulated concrete pore solution. *Surf. Coat. Technol.* **2008**, *202*, 1526−1542.

(23) Asif, A.; Shi, W.; Shen, X.; Nie, K. Physical and thermal properties of UV curable waterborne polyurethane dispersions incorporating hyperbranched aliphatic polyester of varying generation number. *Polymer* **2005**, *46*, 11066−11078.

(24) Asif, A.; Shi, W. UV curable waterborne polyurethane acrylate dispersions based on hyperbranched aliphatic polyester: Effect of molecular structure on physical and thermal properties. *Polym. Adv. Technol.* **2004**, *15*, 669−675.

(25) Asif, A.; Huang, C.; Shi, W. Structure−property study of waterborne, polyurethane acrylate dispersions based on hyperbranched aliphatic polyester for UV-curable coatings. *Colloid Polym. Sci.* **2004**, *283*, 200−208.
(26) Álvarez-Chávez, C. R.; Edwards, S.; Moure-Eraso, R.; Geiser, K. Sustainability of bio-based plastics: General comparative analysis and recommendations for improvement. *J. Clean. Prod.* **2012**, *23*, 47−56.
(27) Tian, H.; Wang, Y.; Zhang, L.; Quan, C.; Zhang, X. Improved flexibility and water resistance of soy protein thermoplastics containing waterborne polyurethane. *Ind. Crops Prod.* **2010**, *32*, 13−20.
(28) Van Buren, J. P.; Robinson, W. B. Formation of complexes between protein and tannic acid. *J. Agric. Food Chem.* **1969**, *17*, 772−777.
(29) Rana, V.; Das, M. K.; Gogoi, S.; Kumar, V. Multifunctional properties of polysaccharides from Dalbergia sissoo, Tectona grandis and Mimosa diplotricha. *Carbohydr. Polym.* **2014**, *102*, 341−350.
(30) Barua, S.; Das, G.; Aidew, L.; Buragohain, A. K.; Karak, N. Copper−copper oxide coated nanofibrillar cellulose: A promising biomaterial. *RSC Adv.* **2013**, *3*, 14997−15004.
(31) Gogoi, S.; Barua, S.; Karak, N. Biodegradable and thermostable synthetic hyperbranched poly(urethane-urea)s as advanced surface coating materials. *Prog. Org. Coat.* **2014**, *77*, 1418−1427.
(32) Pramanik, S.; Konwarh, R.; Sagar, K.; Konwar, B. K.; Karak, N. Bio-degradable vegetable oil based hyperbranched poly(ester amide) as an advanced surface coating material. *Prog. Org. Coat.* **2013**, *76*, 689−697.
(33) Lomölder, R.; Plogmann, F.; Speier, P. Selectivity of isophorone diisocyanate in the urethane reaction influence of temperature, catalysis, and reaction partners. *J. Coating. Technol.* **1997**, *69*, 51−57.
(34) Anderson, R. A.; Broadhurst, C. L.; Polansky, M. M.; Schmidt, W. F.; Khan, A.; Flanagan, V. P.; Schoene, N. W.; Graves, D. J. Isolation and characterization of polyphenol type-A polymers from cinnamon with insulin-like biological activity. *J. Agric. Food Chem.* **2004**, *52*, 65−70.
(35) Wattamwar, P. P.; Mo, Y.; Wan, R.; Palli, R.; Zhang, Q.; Dziubla, T. D. Antioxidant activity of degradable polymer poly(trolox ester) to suppress oxidative stress injury in the cells. *Adv. Funct. Mater.* **2010**, *20*, 147−154.
(36) Pospíšil, J. Mechanistic action of phenolic antioxidants in polymers—A review. *Polym. Degrad. Stab.* **1988**, *20*, 181−202.
(37) Howard, G. T. Biodegradation of polyurethane: A review. *Int. Biodeterior. Biodegrad.* **2002**, *49*, 245−252.

Composites Science and Technology 118 (2015) 39–46

Contents lists available at ScienceDirect

Composites Science and Technology

journal homepage: http://www.elsevier.com/locate/compscitech

High performance luminescent thermosetting waterborne hyperbranched polyurethane/carbon quantum dot nanocomposite with *in vitro* cytocompatibility

Satyabrat Gogoi [a], Manishekhar Kumar [b], Biman B. Mandal [b], Niranjan Karak [a, *]

[a] Advanced Polymer and Nanomaterial Laboratory, Center for Polymer Science and Technology, Department of Chemical Sciences, Tezpur University, Napaam 784028, Assam, India

[b] Biomaterial & Tissue Engineering Laboratory, Department of Biosciences and Bioengineering, Indian Institute of Technology, Guwahati, 781039, Assam, India

ARTICLE INFO

Article history:
Received 16 June 2015
Received in revised form
7 August 2015
Accepted 10 August 2015
Available online 11 August 2015

Keywords:
A. Polymers
A. Nano particles
A. Nano composites
B. Mechanical properties
B. Thermal properties

ABSTRACT

Development of high performance and benign polymeric material still remains a challenge across the globe. Comforting the prevailing challenge, we report *in situ* and *ex situ* fabrication of tannic acid based waterborne hyperbranched polyurethane (WPU) nanocomposites as fluorescent and cytocompatible materials by incorporating various weight percentages (0.5, 1.0 and 1.5 wt%) of carbon quantum dot (CQD). CQD was synthesized from corms of *Colocasia esculenta* having an average size 3.2 nm. The waterborne nanocomposites were cured by using glycerol based hyperbranched epoxy in the presence of fatty acid based poly(amido amine) to obtain the desired thermosets. FTIR, Raman, UV–visible spectroscopy, XRD study and HRTEM analyses confirmed the structural changes occurred upon interaction of CQD with WPU. The thermosets showed a good photo luminescent behavior, which confirmed efficiency of the polymer matrix to prevent solid state quenching. The thermosetting nanocomposites exhibited dose dependent improvement of mechanical (tensile strength ~4.6 fold, toughness ~4.2 fold, scratch hardness> 2 fold, impact resistance> 1.25 fold compared to thermoplastic pristine WPU) and thermal stability (maximum 28 °C enhancement). The thermosetting films were found to be biocompatible for *in vitro* adhesion, proliferation and differentiation of MG 63 osteoblast cells with good cell viability.

1. Introduction

Of late, nanotechnology based polymeric composites paved a new paradigm to material research owing to their huge viability for a wide range of advanced applications [1–5]. It has been observed that incorporation of even a minute quantity of nano filler can lift up the various material properties dramatically [6]. The substantial differences in physico–chemical properties compare to the bulk phase lead to the unique behavior of nanomaterials, which can be exploited to design polymeric nanocomposites with tunable properties [7].

In this context, carbonaceous nanostructures have been extensively used by virtue of tunable physical, chemical, electrical and biological properties [8]. Most recently, carbon quantum dot (CQD) has shown remarkable promises in this regard [9]. CQD is the most recent addition to the carbonaceous nanomaterial family having dimension less than 10 nm. CQD exhibits excellent nano state aqueous solubility, exciting optical properties and profound biocompatibility [10–12]. The phenomenal properties of CQD, primarily attributed to quantum confinement effect, conferred it a special niche in domains ranging from biomedical, photocatalytic to optoelectronic applications [13–16]. Moreover, CQD provides facile preparative route by using nontoxic chemicals, environmentally benign solvents and renewable precursors which are consistent to the tenets of green chemistry [9,17]. CQD, thus, appears to be a suitable candidate amidst all other owing to its numerous advantages.

Henceforth, the authors here in like to present *in situ* and *ex situ* fabrication of hyperbranched polyurethane/carbon dot nanocomposite. Recently, we reported tannic acid based biodegradable waterborne hyperbranched polyurethane (WHPU) as an eco-friendly material [18]. Here, it is pertinent to mention that the

* Corresponding author.
E-mail address: karakniranjan@gmail.com (N. Karak).

http://dx.doi.org/10.1016/j.compscitech.2015.08.010
0266-3538/

developed material by virtue of attributes like low VOC content, bio-based origin and profound bio-activity (anti-oxidant behavior and hemocompatibility) has the prospective to address a cocktail of challenges ranging from sustainability to environmental footprints. Therefore, judicious inclusion of CQD and WHPU onto the same matrix appears to pave direction towards the development of a sustainable and eco-friendly material. Besides the environmental benefits, the approach of using CQD to fabricate WHPU seems to credit several other merits as well. The aromatic carbonized structure of CQD with highly polar peripheral groups conferred a strong physico–chemical interaction with the polymer matrix which consequences the enhancement of mechanical properties. On the other hand, quantum size dimension and good compatibility with the polymer matrix may help to retain transparency of the pristine films; which is difficult to achieve with other carbonaceous nano structures. The optical emission under different wavelength of UV light may help to design different optoelectronic devices e.g. light emitting diode, UV detector or anti-counterfeiting agent [19,20]. Further, CQD has the potentiality to promote biocompatibility of the nanocomposite system for allied biomedical applications. Literature cited very few reports on CQD/polymer nanocomposite [21–24]. On the other hand, Luo et al. reported CdTe quantum dot based waterborne polyurethane nanocomposite with enhanced photoluminescence behavior [25]. Hence, an effort has been made to study CQD/WHPU nanocomposite using different characterization techniques with an attention to evaluate *in vitro* cytocompatibility with osteoblast cell line.

2. Experimental

2.1. Materials

Isophorone diisocyanate (IPDI, Aldrich, Germany), Poly(ethylene glycol) with M_n 600 g/mol (PEG-600, Merck, India), 1,4 butane diol (BD, Merck, India), tannic acid (TA, Sigma–Aldrich, Belgium), 2, 2-Bis(hydroxymethyl) propionic acid (BMPA, Aldrich, Germany), triethylamine (TEA, Merck, India), epichlorohydrin (Merck, India), bis-phenol A (Merck, India), poly(amido amine) (PAA, HY840, Ciba Geigy, amine value 5–7 eq./kg) and tetrahydrofuran (THF, Merck, India) were used. Corms of *Colocasia esculenta* was collected from the Tezpur University, India campus. Glycerol based Hyperbranched epoxy (HBE) was prepared by following the method described elsewhere [26]. The terms WPU and EPU were used to define the pristine waterborne hyperbranched polyurethane and epoxy cured polyurethane thermoset respectively.

2.2. Fabrication of thermosetting waterborne hyperbranched polyurethane/carbon quantum dot nanocomposite (PNC)

Hyperbranched polyurethane/CQD nanocomposites were fabricated by using both *in situ* and *ex situ* techniques. For *in situ* fabrication, required amount of IPDI, PEG 600 and BMPA (−NCO to −OH ratio is 1.5) were reacted at 80–90 °C for 2 h. In the next step, THF solution of BD and TA were added and further reaction was carried out at 65–70 °C for another 3.5 h. Then CQD was introduced and the reaction was continued for 1.5 h. It was followed by neutralization of −COOH groups at room temperature by the addition of TEA. Finally, water was added at a very slow rate. THF was recovered under reduced pressure. All the steps were carried out under the inert atmosphere of nitrogen with constant mechanical agitation. Thermosetting nanocomposite was obtained by mixing this polyurethane with glycerol based HBE (20 wt%) and fatty acid based PAA (10 wt%) using ultra-sonication (@ 60% amplitude and 0.5 cycle for 20 min) followed by curing at 100 °C for 45 min. For *ex situ* fabrication, the same method was employed, except CQD was introduced in the curing step instead of incorporating it in the polymerization step. Three different nanocomposites *viz.* PNC0.5, PNC1.0 and PNC1.5 were prepared by both *in situ* and *ex situ* fabrications using 0.5, 1.0 and 1.5 wt% of CQD respectively. Characterization and properties were evaluated by using different techniques (Supplementary information).

2.3. Biological assessment of PNC

Osteoblast cell (MG63 cell) proliferation on the PNC films was examined by Alamar blue assay (Invitrogen, USA) at the 1st, 6th and 9th day following the manufacturers' protocol ($n = 4$). Whereas, cell viability and call adherence was studied by Live/Dead assay after 7 days of culture (Sigma–Aldrich, USA). Osteogenic differentiation of MG 63 cells on the PNC films was assessed by monitoring deposition of calcium minerals after staining with Alizarin Red S stain (Sigma–Aldrich, USA). The detail experimental procedure is provided in the Supplementary information Section.

3. Results and discussion

3.1. Synthesis and characterization of CQD

CQD is synthesized by heating the aqueous extract of corms of *C. esculenta* as a carbohydrate rich bio-precursor (Synthesis is provided in the Supplementary information Section). As demonstrated in earlier work, CQD was formed by the carbonization of different carbohydrates present in the aqueous ethanolic solution [17,27–30]. The size and morphology of the synthesized CQD were studied by TEM analysis. The TEM image as depicted in Fig. 1a confirmed the formation of nanoparticles with almost spherical shape, having dimension 2.2–5.1 nm range. Statistical evaluation of size distribution (Fig. 1b) revealed that the mean size of the particles was 3.2 nm. HRTEM micrograph showed a lattice spacing of 0.341 nm which is close to the (002) lattice spacing of graphite (Fig. 2a, d). The Raman spectrum of CQD exhibited two distinct bands *viz.* D and G bands at 1362 and 1582 cm^{-1} respectively as shown in Fig. 3a (i). The appearance of D band indicates the presence of disorder to the graphitic structure. Such disorder originates from the presence of different oxygen functional groups in CQD. However, I_D/I_G ratio of 0.57 indicates the formation of near pristine graphitic structure in the form of CQD. The 2D peak at 2765 cm^{-1} can be ascribed to the multilayered structure of CQD. This is further supported by TEM images. On the other hand, XRD pattern displayed a broad peak at around $2\theta = 23.47°$, (Fig. 3b (i)) which indicated higher interlayer spacing and poor crystallinity of CQD compared to pristine graphitic carbonaceous structure. Generation of oxygenous groups contributes towards amorphous behavior of CQD. Characteristic FTIR absorption frequencies at 3465, 2975, 1680, 1602, 1542 and 1246 cm^{-1} confirmed the presence of −OH, −CH, −C=O, −C=C− and −C−O−C− groups respectively (Fig. 3c (i)). Elemental analysis of CQD showed the presence of C and O in a weight ratio of 61.47:36.53 (Fig. 1c). In the UV–visible spectrum, an absorption peak at around 265 nm was observed for CQD (Fig. 3d (i)) whereas, the absorption peak for *C. esculenta* was witnessed at 277 nm.

3.2. Fabrication and characterization of PNC

The CQD nanocomposites of WPU were fabricated by *in situ* as well as *ex situ* polymerization techniques using 0.5, 1.0 and 1.5 wt% of the nanomaterial. Different chemical functionalities present are established by FTIR spectroscopy as depicted in Fig. 3c (ii and iii). Various oxygenous functional groups of CQD possess an inherent tendency to interact with polyurethane or polyurethane precursors either by covalently or non-covalently as shown in Scheme 1. Such

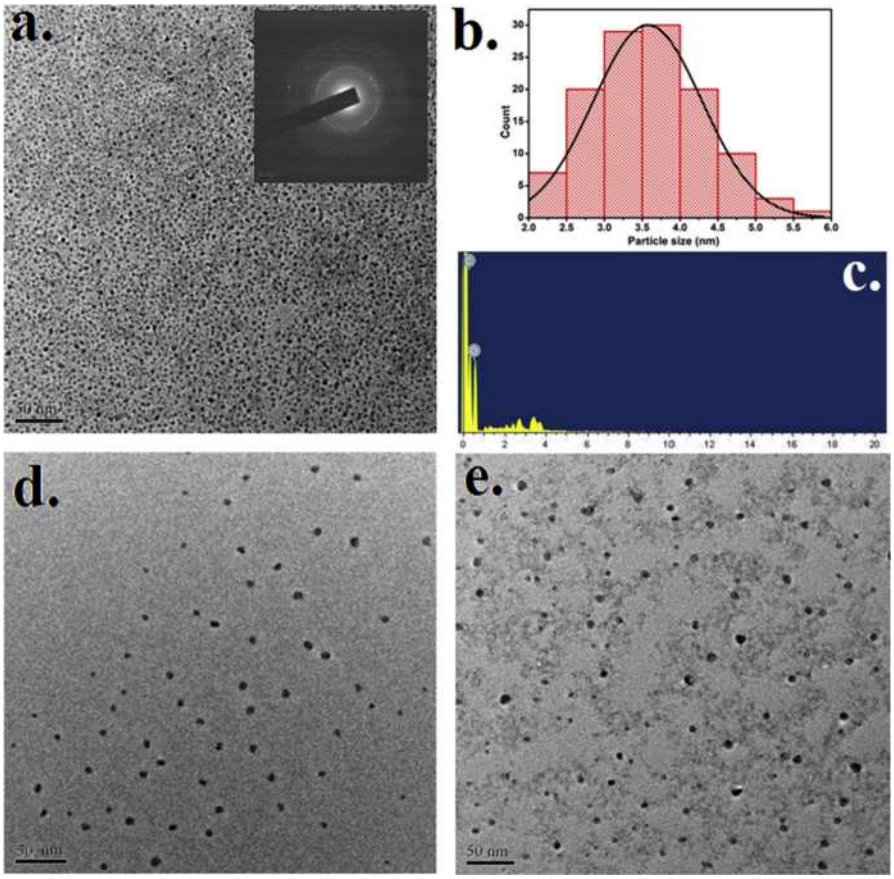

Fig. 1. TEM image of CQD (in set SAED pattern of CQD), b. Particle size distribution of CQD, c. EDX spectrum of CQD, d. TEM image showing distribution of CQD in PNC1.5 (*ex situ*) and e. TEM image showing distribution of CQD in PNC1.5 (*in situ*).

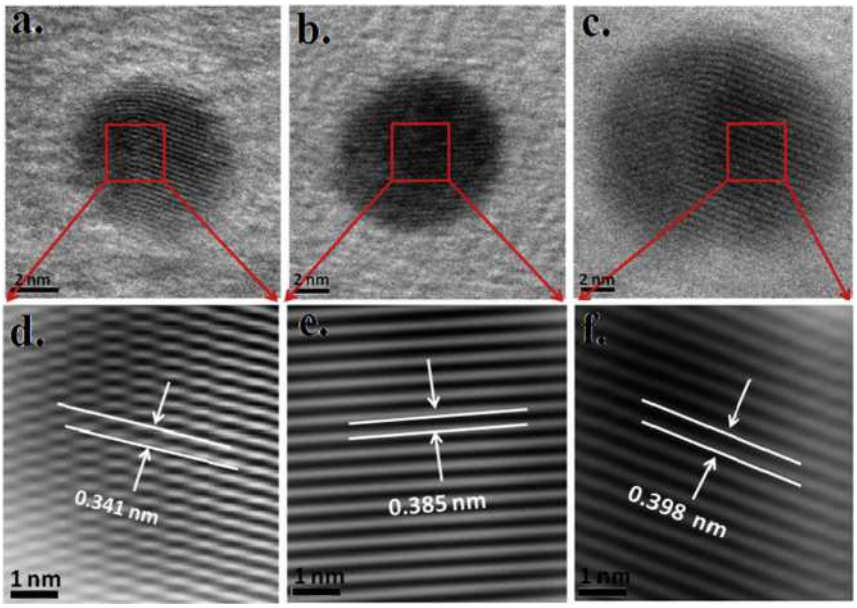

Fig. 2. HRTEM images of a. CQD, b. PNC1.5 (*ex situ*), c. PNC1.5 (*in situ*) and IFFT of d. CQD, e. PNC1.5 (*ex situ*) and f. PNC1.5 (*in situ*).

interactions play the central role towards the homogeneous distribution of nanomaterial over the polymer matrix. Moreover, in many instances lake of proper solubility of nanomaterial and polymer in the reaction medium create barrier. In this context, use of CQD and WPU are an apt option because of their excellent dispersibility in aqueous phase. TEM image of PNC1.5 depicted in Fig. 1d and e) confirmed a uniform sharing of CQD even at the highest nanomaterial loading. HRTEM and IFFT images (Fig. 2a–f)

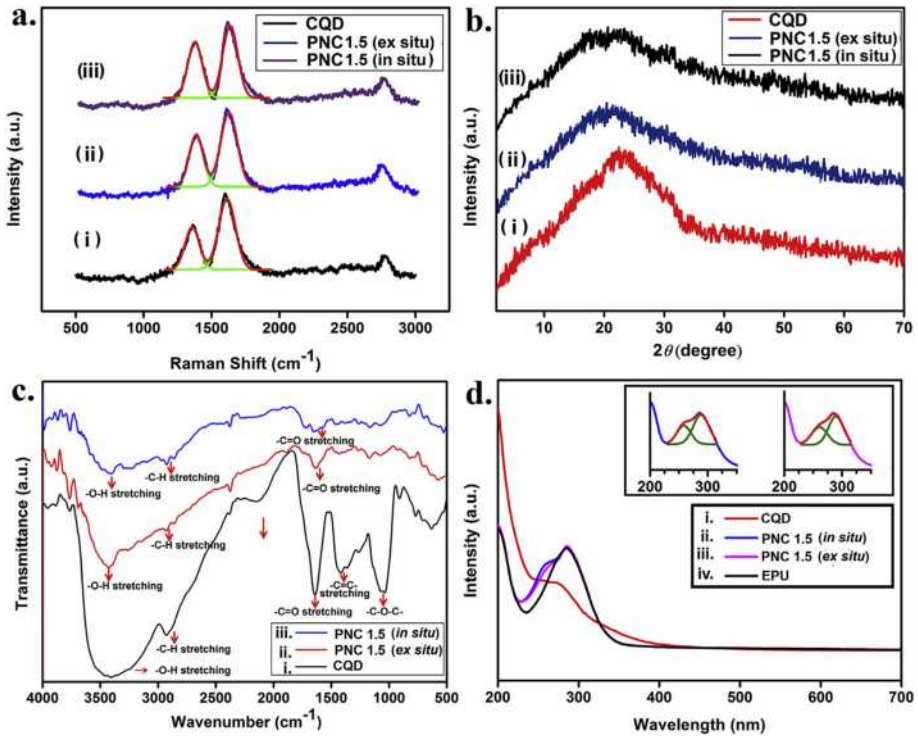

Fig. 3. Raman spectra of (i) CQD, (ii) PNC1.5 (*ex situ*) and (iii) PNC1.5 (*in situ*); b. XRD patterns of (i) CQD, (ii) PNC1.5 (*ex situ*) and (iii) PNC1.5 (*in situ*); c. FTIR spectra of (i) CQD, (ii) PNC1.5 (*ex situ*) and (iii) PNC1.5 (*in situ*); d. UV–visible spectra of (i) CQD, (ii) PNC1.5 (*ex situ*) and (iii) PNC1.5 (*in situ*) and (iv) EPU (in set deconvoluted spectra of PNC1.5 (*ex situ*) and PNC1.5 (*in situ*)).

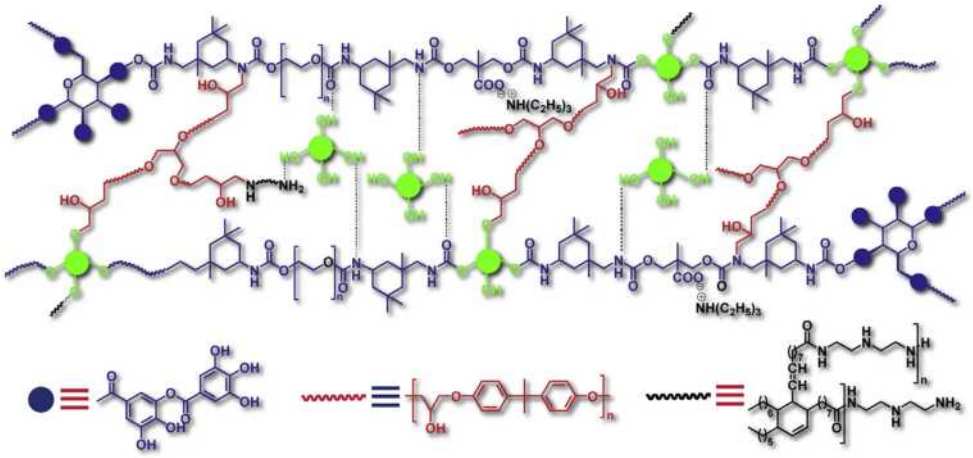

Scheme 1. Thermosetting *in situ* WPU/CQD nanocomposite (for thermosetting *ex situ* WPU/CQD nanocomposite covalent interaction of CQD with the polymer matrix are not present).

revealed that the layer spacing of CQD increased after fabrication, which was more pronounced for *in situ* PNC1.5 (0.398 nm) compared to the *ex situ* counterpart (0.385 nm). Participation of CQD in chemical reaction might reduce the crystallinity of poorly crystalline CQD further. This may increase the interlayer spacing of CQD after the formation of nanocomposite. Moreover, as CQD has a layered structure, intercalation may happen upon formation of the nanocomposite. Raman spectra of PNC1.5 (*ex situ* and *in situ*) as shown in Fig. 3a (ii and iii) displayed both D and G bands at 1344 and 1589 cm^{-1} similar to that of CQD. However, the most obvious difference marked was the increased intensity of D band compared to the same of pristine CQD. This originated from additional defect or disorder created in CQD structure during fabrication of the nanocomposites. This implies definite interaction between CQD and the polymer. The XRD pattern of PNC1.5 (*ex situ* and *in situ*) followed a much weakly intense and broad peak as shown in Fig. 3b (ii and iii). This could be again attributed to the disorderliness of the atoms created by the strong interactions between CQD and polymer chains. The UV–visible spectra of PNCs depicted in Fig. 3d (taken before curing) showed a doublet. Deconvolution of the same gives an idea about the existence of two overlapping peaks; the intense peak at 284 nm is for catechol fraction of the polymer, while slightly weakly intense peak at 262 nm is for CQD (inset to Fig. 3d).

3.3. Optical properties

The nanocomposite films exhibit fascinating optical properties with good transparency which is difficult to achieve with other

carbonaceous nanomaterials (Fig. S1 of Supplementary information). This can be attributed to the quantum size of the nanoparticles and their excellent dispersion in the polymer matrix. On the other hand, the changes in color of both CQD and PNC were examined under visible, short UV (254 nm) and long UV (365 nm) region. The original light brown color of CQD changed to green and deep blue color (in the web version) under the exposure of long and short UV light respectively (Fig. 4d). Similar color change was perceived in case of PNC films as well (Fig. 4f–g). Detail optical properties of CQD and PNC were studied by PL spectroscopy as depicted in Fig. 4a–c. An excitation wavelength dependent photoluminescence behavior was witnessed with shifting of the emission peak towards higher wavelength with increase in excitation wavelength. This can be ascribed to the existence of different surface states and size dispersion of CQD. Quantum yield was measured by using quinine sulfate as the reference. Quantum yields were found as 10.42, 7.97 and 6.82% for CQD, PNC1.5 (*in situ*) and PNC1.5 (*ex situ*) respectively. The better quantum yield value of PNC1.5 (*in situ*) compared to PNC1.5 (*ex situ*) is due to better dispersion of CQD in the former than in the later. In contrary to CQD, a broad emission peak was observed for the PNC films as depicted in Fig. 4b–c. This can be attributed to the inner filter effect, which results from the re-absorption of emitted light in a condensed matter. Short wavelength light emitted by PNC may be absorbed by CQD in the matrix. This may result re-emission of red shifted long wavelength light. This is a repeated process which occurs until the emitted light passes through the film completely. This results the cut-off of short wavelength emission followed by enhancement of long wavelength emission. As a result, the PL intensity of the existing peaks gradually diminishes and peaks at higher wavelength simultaneously evolve resulting in their broadening. In this vein, waterborne polymer matrix seems to play an important role by providing mechanical support as well as uniform dispersion to prevent solid state quenching of CQD. Moreover, similar to CQD, PNC films also exhibited wavelength dependent emission and concentration dependent intensity. Such highly photo luminescent material can be used to fabricate novel engineered material for bio-photonic as well as opto-electronic devices for their allied applications. In Fig. 4e we demonstrated anti-counterfeiting application of the PNC.

3.4. Mechanical properties

Mechanical properties of WPU, EPU and PNC are tabulated in Table 1. From the results, we witnessed an excellent enhancement of mechanical properties of the nanocomposites even at the lowest loading of CQD compared to WPU and EPU. The major drawbacks of epoxy modified polyurethane thermoset are the decrease in elongation at break value and lose of flexibility. In the current study we witnessed ~44% decrease in elongation at break value of the pristine polymer after modification. But, the most interestingly this property was improved after the formation of nanocomposites by 1.6 fold (maximum). This may originate from the layered structure of CQD. Dose dependent enhancement of tensile strength was also perceived by the fabrication of nanocomposites. The nanocomposites exhibited high values of scratch hardness and impact resistance. However, we could not quantify the exact values as both scratch hardness and impact resistance crossed the limiting values of the instruments used. Nevertheless, stress–strain profiles (shown in Fig. S2 of Supplementary information) and measurement of toughness clearly showed an excellent gain in mechanical performance after the formation of nanocomposites. The improved performance of the nanocomposites can be attributed to the factors such as excellent dispersion, strong interfacial interaction and nano

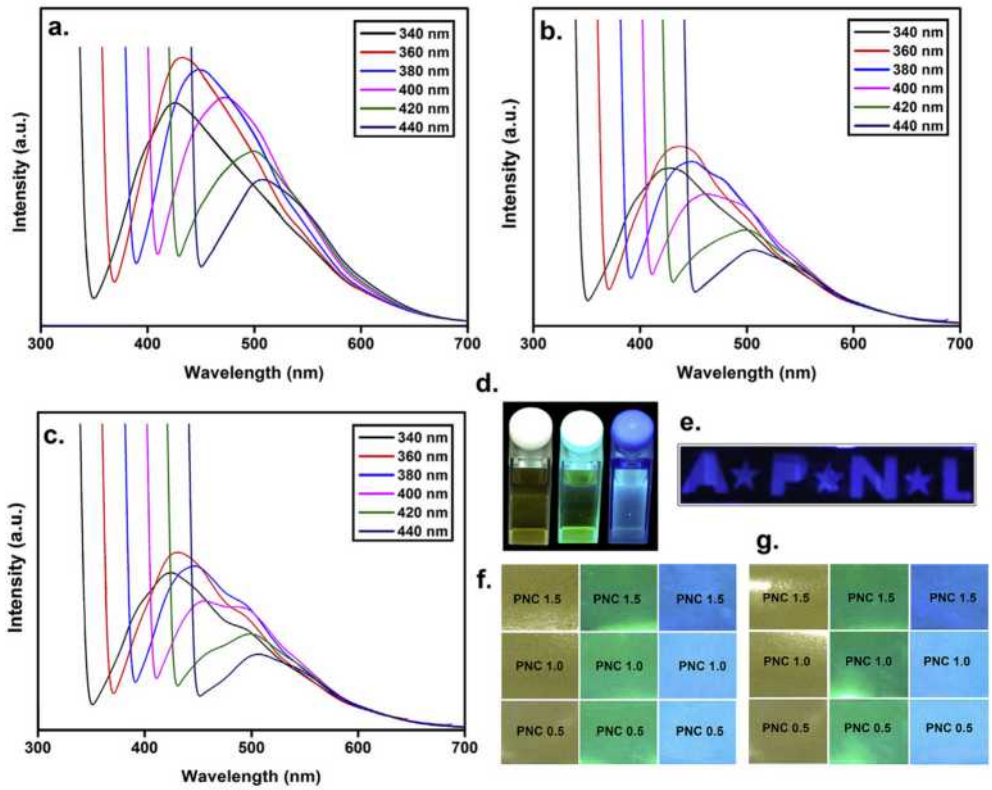

Fig. 4. PL spectra of a. CQD, b. PNC1.5 (*ex situ*) and c. PNC1.5 (*in situ*); d. Luminescence of CQD under visible, short UV (254 nm) and long UV (365 nm), e. Demonstration of PNC as a security mark, f. PNCs (*ex situ*) and g. PNCs (*in situ*) under visible, short UV (254 nm) and long UV (365 nm).

Table 1
Mechanical properties of nanocomposites.

Properties	WPU	EPU	*In situ*			*Ex situ*		
			PNC0.5	PNC1.0	PNC1.5	PNC1.0	PNC 0.5	PNC1.5
Tensile strength (MPa)	5.8 ± 0.2	16.45 ± 0.35	19.42 ± 0.23	25.42 ± 0.32	28.58 ± 0.27	17.94 ± 0.45	20.46 ± 0.35	23.42 ± 0.23
Elongation at break (%)	437 ± 5	210 ± 2	265 ± 3	289 ± 2	340 ± 3	245 ± 3	262 ± 1	305 ± 3
Toughness[a] (MPa)	18.84	30.52	47.66	63.49	75.51	36.85	44.62	55.53
Scratch hardness[b] (kg)	5.0 ± 0.2	10	10	10	10	10	10	10
Impact resistance[c] (cm)	80 ± 2	100	100	100	100	100	100	100
Bending[d] (mm)	<1	<2	<1	<1	<1	<1	<1	<1
Gloss (60°)	84.52	95.24	96.74	96.97	98.49	95.45	96.89	97.42

[a] Calculated by integrating the area under stress–strain curve.
[b] Limit of the instrument for scratch hardness was 10 kg (maximum).
[c] Limit of the instrument for impact resistance was 100 cm (maximum).
[d] Limit of the mandrel diameter was 1 mm (minimum).

scale morphology of CQD. CQD with carbonized core structure and large peripheral polar functional groups can provide stiffness and strong interactions within the polymer matrix, which play the vital role towards the improved mechanical properties of PNC. On the other hand, *in situ* PNC exhibited better mechanical properties than the *ex situ* one, by virtue of better dispersion and strong interactions as discussed in the characterization section.

3.5. Thermal properties

In order to evaluate the thermal stability of PNC, thermal gravimetric analysis was performed. We found improved thermostability after the formation of the nanocomposite (Fig. 5), which was consistent with the loading of CQD. The increased thermostability of the nanocomposites can be attributed to high cross-linking density and secondary interactions imparted by CQD with the polymer chains. In a highly cross-linked network, molecular chain excitation and motion generated during exposure to thermal energy is prohibited significantly which makes the degradation process energy consuming. CQD by virtue of large number of functional groups participated in the cross-linking reaction (Scheme 1). This results restrictions in the macromolecular chain motion making the system more rigid. Consequently, the process of bond breaking becomes more heat expensive resulting greater thermostability of nanocomposites compared to EPU. Secondary interactions like hydrogen bonding and polar–polar interactions also play the vital role towards the enhancement of thermal properties. Almost similar type of improvement was noticed for both the *in situ* and *ex situ* PNC.

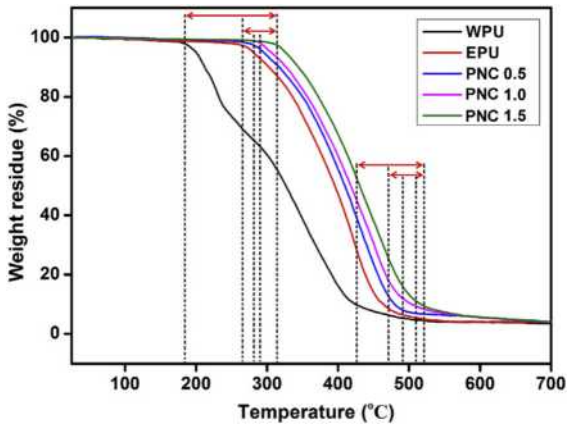

Fig. 5. TGA thermograms of WPU, EPU and *in situ* PNC0.5, PNC1.0 and PNC1.5.

3.6. Biological assessment of PNC film

Cell proliferation assay was carried out with MG63 cell line in order to judge the potentiality of the PNC films as a biomaterial. The observed Alamar blue reduction value which directly relates to cellular metabolism and cell proliferation at a given point of time suggested that the CQD impregnated films are cytocompatible for biological applications [31,32]. In comparison to day 01, Alamar blue assay revealed ~20% increase in cell number on WPU and PNC0.5 and ~30% on PNC1.0 and PNC1.5 on day 09 of culture (Fig. 1). However, no statistical significance was observed between the groups ($p > 0.05$). From results it may be inferred that the polyurethane, a well reputed biomaterial, which is the main component of the membranes aids to cell adhesion and proliferation [33]. Additionally CQD which has been incorporated into films is reported to be a cytocompatible material used in making composites with enhanced physico–chemical and biological properties [34,35]. The incorporation of CQD in polyurethane membrane led to better cell proliferation on PNC1.0 and PNC1.5 compare to WPU film (Fig. 6). The study confirmed polyurethane/CQD nanocomposite films reported here in showed enhanced cellular proliferation clearly suggesting the suitability of these nanocomposites for bone regeneration and other allied biological applications. On the other hand, Live/Dead assay indicated attachment and viability of MG 63 cells onto membranes. Cells maintained their native morphology and were distributed uniformly on all films (Fig. 7 (a), (b), (c) and (d)). Proliferating cells were found to form clusters on

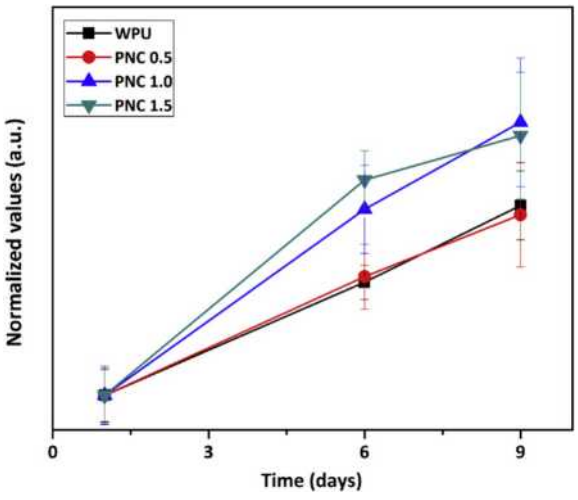

Fig. 6. Alamar blue cell proliferation assay showing MG 63 osteosarcoma cell proliferation on all the membranes. Data represented as the average ± standard deviation.

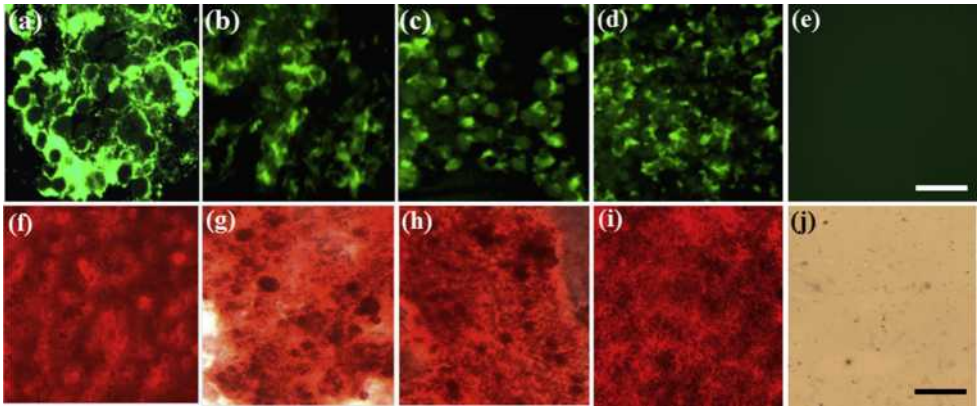

Fig. 7. Fluorescent microscopic images showing MG 63 cells growing on (a) WPU, (b) PNC0.5, (c) PNC1.0, (d) PNC1.5 after seven days of culture; Light microscopic images of (f) WPU (g) PNC0.5, (h) PNC1.0, (i) PNC1.5 showing mineralized deposits in the form of nodule due to osteogenic differentiation of MG 63 cells. Microscopic image (e) and (j) represents PNC1.5 film without cell. Scale bar represents 100 μm.

the films which is further expected to help in good cell to cell signaling leading to enhanced extracellular matrix (ECM) secretion and deposition. Enhancement of ECM formation overtime is very important in the context of tissue engineering as high ECM would led to mature tissues similar as in native state. Live/Dead result was found to be in agreement with the Alamar blue cell proliferation results suggesting film cytocompatibility. Alizarin Red S staining was performed to confirm the hallmark characteristic of osteogenic differentiation i.e. mineral deposition on the films. Films seeded with MG 63 cells for 10 days in osteogenic media were assessed for calcium deposition. Microscopic analysis showed enhanced osteogenic differentiation on films resulting in extensive extracellular mineralization in the form of deposited nodules. Intense red Alizarin Red S staining of nodules all over the films confirms extensive mineralization (Fig. 7 (f), (g), (h), (i)). These granules were formed in patches as area of diffused and nodular mineralization throughout the films. This clearly suggests bone forming potential of these nanocomposite films.

4. Conclusions

Thus, the present study demonstrated *in situ* and *ex situ* fabrication of carbon dot/thermosetting waterborne hyperbranched polyurethane nanocomposite with biocompatible attributes for the first time. The study witnessed improvement of material properties of the pristine polymer upon formation of nanocomposites in multiple aspects especially in case of *in situ* fabricated nanocomposite. High mechanical properties and thermostability of the nanocomposites can form the genuine solution of the inferior performance of waterborne polyurethane. On the other hand, utilization of benign solvent system as well as bio-based raw materials for the development of both the nanomaterial and polymer justified the sustainability and eco-friendliness of the developed nanocomposites. The biological assessment particularly osteoblast proliferation and differentiation revealed a cytocompatible material which had the potentiality to be used in allied biomedical applications.

Acknowledgments

The work is financially supported by Government of India under the following grants (DBT- BT/235/NE/TBP/2011; DST- BT/FT/LS-213/2012 and ICMR- 5/7/771/12-RCH). The authors would like to express their gratitude to SAIF, Shillong and Mr. Joston Nongkynrih for TEM imaging. The authors also acknowledged Mr. Tridip Ranjan Chetia, IIT Guwahati for his help in TEM analysis.

Appendix A. Supplementary information

Supplementary information related to this article can be found at http://dx.doi.org/10.1016/j.compscitech.2015.08.010.

References

[1] D.R. Paul, L.M. Robeson, Polymer nanotechnology: nanocomposites, Polymer 49 (2008) 3187–3204.
[2] J.H. Koo, Polymer Nanocomposites, McGraw-Hill Professional Pub, 2006.
[3] M.S. Scholz, J.P. Blanchfield, L.D. Bloom, B.H. Coburn, M. Elkington, J.D. Fuller, M.E. Gilbert, S.A. Muflahi, M.F. Pernice, S.I. Rae, J.A. Trevarthen, S.C. White, P.M. Weaver, I.P. Bond, The use of composite materials in modern orthopaedic medicine and prosthetic devices: a review, Compos. Sci. Technol. 71 (2011) 1791–1803.
[4] H.C. Kuan, C.C.M. Ma, W.P. Chang, S.M. Yuen, H.H. Wu, T.M. Lee, Synthesis thermal mechanical and rheological properties of multiwall carbon nanotube/waterborne polyurethane nanocomposite, Compos. Sci. Technol. 65 (2005) 1703–1710.
[5] T. Ramanathan, A.A. Abdala, S. Stankovich, D.A. Dikin, M. Herrera-Alonso, R.D. Piner, D.H. Adamson, H.C. Schniepp, X. Chen, R.S. Ruoff, S.T. Nguyen, I.A. Aksay, R.K. Prud'Homme, L.C. Brinson, Functionalized graphene sheets for polymer nanocomposites, Nat. Nanotechnol. 3 (2008) 327–331.
[6] F. Hussain, M. Hojjati, M. Okamoto, R.E. Gorga, Polymer- matrix nanocomposites, processing, manufacturing, and application: an overview, J. Compos. Mater. 40 (2006) 1511–1575.
[7] M. Mahmoudi, P. Stroeve, A.S. Milani, A. Arbab, Superparamagnetic Iron Oxide Nanoparticles for Biomedical Applications, Nova Science Publishers, Inc, 2010.
[8] M.S. Mauter, M. Elimelech, Environmental applications of carbon-based nanomaterials, Environ. Sci. Technol. 42 (2008) 5843–5859.
[9] F. Du, M. Zhang, X. Li, J. Li, X. Jiang, Z. Li, Y. Hua, G. Shao, J. Jin, Q. Shao, Economical and green synthesis of bagasse-derived fluorescent carbon dots for biomedical applications, Nanotechnology 25 (2014) 315702.
[10] S.Y. Lim, W. Shen, Z. Gao, Carbon quantum dots and their applications, Chem. Soc. Rev. 44 (2015) 362–381.
[11] M. Bacon, S.J. Bradley, T. Nann, Graphene quantum dots, Part. Part. Syst. Charact. 31 (2014) 415–428.
[12] S.N. Baker, G.A. Baker, Luminescent carbon nanodots: emergent nanolights, Angew. Chem. Int. Ed. 49 (2010) 6726–6744.
[13] M.P. Sk, A. Jaiswal, A. Paul, S.S. Ghosh, A. Chattopadhyay, Presence of amorphous carbon nanoparticles in food caramels, Sci. Rep. 2 (2012).
[14] H.X. Wang, J. Xiao, Z. Yang, H. Tang, Z.T. Zhu, M. Zhao, Y. Liu, C. Zhang, H.L. Zhang, Rational design of nitrogen and sulfur co-doped carbon dots for efficient photoelectrical conversion applications, J. Mater. Chem. A 3 (2015) 11287–11293.
[15] Y. KyungáJung, Sweet nanodot for biomedical imaging: carbon dot derived from xylitol, RSC Adv. 4 (2014) 23210–23213.
[16] R. Narayanan, M. Deepa, A.K. Srivastava, Förster resonance energy transfer and carbon dots enhance light harvesting in a solid-state quantum dot solar cell, J. Mater. Chem. A 1 (2013) 3907–3918.
[17] B. De, N. Karak, A green and facile approach for the synthesis of water soluble fluorescent carbon dots from banana juice, RSC Adv. 3 (2013) 8286–8290.
[18] S. Gogoi, N. Karak, Biobased biodegradable waterborne hyperbranched polyurethane as an ecofriendly sustainable material, ACS Sustain. Chem. Eng. 2

(2014) 2730–2738.
[19] L. Zhou, B. He, J. Huang, Amphibious fluorescent carbon dots: one-step green synthesis and application for light-emitting polymer nanocomposites, Chem. Commun. 49 (2013) 8078–8080.
[20] W. Kwon, S. Do, J. Lee, S. Hwang, J.K. Kim, S.W. Rhee, Freestanding luminescent films of nitrogen-rich carbon nanodots toward large-scale phosphor-based white-light-emitting devices, Chem. Mater. 25 (2013) 1893–1899.
[21] Y. Hao, Z. Gan, J. Xu, X. Wu, P.K. Chu, Poly (ethylene glycol)/carbon quantum dot composite solid films exhibiting intense and tunable blue–red emission, Appl. Surf. Sci. 311 (2014) 490–497.
[22] B. De, B. Voit, N. Karak, Transparent luminescent hyperbranched epoxy/carbon oxide dot nanocomposites with outstanding toughness and ductility, ACS Appl. Mater. Interfaces 5 (2013) 10027–10034.
[23] P. Zhang, W. Li, X. Zhai, C. Liu, L. Dai, L.W. Liu, A facile and versatile approach to biocompatible fluorescent polymers from polymerizable carbon nanodots, Chem. Commun. 48 (2012) 10431–10433.
[24] A. Konwar, N. Gogoi, G. Majumdar, D. Chowdhury, Green chitosan–carbon dots nanocomposite hydrogel film with superior properties, Carbohydr. Polym. 115 (2015) 238–245.
[25] X. Luo, J. Han, Y. Ning, Z. Lin, H. Zhang, B. Yang, Polyurethane-based bulk nanocomposites from 1-thioglycerol-stabilized CdTe quantum dots with enhanced luminescence, J. Mater. Chem. 21 (2011) 6569–6575.
[26] S. Barua, G. Dutta, N. Karak, Glycerol based tough hyperbranched epoxy: synthesis, statistical optimization and property evaluation, Chem. Eng. Sci. 95 (2013) 138–147.
[27] S. Sahu, B. Behera, T.K. Maiti, S. Mohapatra, Simple one-step synthesis of highly luminescent carbon dots from orange juice: application as excellent bio-imaging agents, Chem. Commun. 48 (2012) 8835–8837.
[28] L. Tang, R. Ji, X. Cao, J. Lin, H. Jiang, X. Li, K.S. Teng, C.M. Luk, S. Zeng, J. Hao, S.P. Lau, Deep ultraviolet photoluminescence of water-soluble self-passivated graphene quantum dots, ACS Nano 26 (2012) 5102–5110.
[29] W. Kwon, S.W. Rhee, Facile synthesis of graphitic carbon quantum dots with size tunability and uniformity using reverse micelles, Chem. Commun. 48 (2012) 5256–5258.
[30] J. Ryu, Y.W. Suh, D.J. Suh, D.J. Ahn, Hydrothermal preparation of carbon microspheres from mono-saccharides and phenolic compounds, Carbon 48 (2010) 1990–1998.
[31] B.B. Mandal, S.C. Kundu, Osteogenic and adipogenic differentiation of rat bone marrow cells on non-mulberry and mulberry silk gland fibroin 3D scaffolds, Biomaterials 30 (2009) 5019–5030.
[32] B.B. Mandal, S. Kundu, Non-mulberry silk gland fibroin protein 3-D scaffold for enhanced differentiation of human mesenchymal stem cells into osteocytes, Acta Biomater. 5 (2009) 2579–2590.
[33] A.T. Stevenson, L.M. Reese, T.K. Hill, J. McGuire, A.M. Mohs, R. Shekhar, L.R. Bickford, A.R. Whittington, Fabrication and characterization of medical grade polyurethane composite catheters for near-infrared imaging, Biomaterials 54 (2015) 168–176.
[34] S.T. Yang, X. Wang, H. Wang, F. Lu, P.G. Luo, L. Cao, M.J. Meziani, J.H. Liu, Y. Liu, M. Chen, Y. Huang, Y.P. Sun, Carbon dots as nontoxic and high-performance fluorescence imaging agents, J. Phys. Chem. C 113 (2009) 18110–181114.
[35] P.C. Hsu, Z.Y. Shih, C.H. Lee, H.T. Chang, Synthesis and analytical applications of photoluminescent carbon nanodots, Green Chem. 14 (2012) 917–920.